Combustion and Flame 245 (2022) 112372

Contents lists available at ScienceDirect

Combustion and Flame

journal homepage: www.elsevier.com/locate/combustflame

Experimental and kinetic modeling study of the laminar burning velocity of NH_3/DME/air premixed flames

Huahua Xiao[a,b,*], Huizhen Li[a]

[a] State Key Laboratory of Fire Science, University of Science and Technology of China, Hefei, Anhui 230027, China
[b] Dalian National Laboratory for Clean Energy, Dalian 116023, China

ARTICLE INFO

Article history:
Received 18 April 2022
Revised 6 September 2022
Accepted 6 September 2022
Available online 23 September 2022

Keywords:
Ammonia
Dimethyl ether
Laminar burning velocity
Kinetic modeling
Elevated pressure

ABSTRACT

Ammonia (NH_3) as a carbon-free fuel and a high-density hydrogen carrier has received significant attention. Co-firing NH_3 with dimethyl ether (DME) is a promising option for overcoming the low reactivity of NH_3. This paper presents an experimental and kinetic modeling study of the laminar burning velocity of NH_3/DME/air mixtures. Experiments were conducted for the full range of DME fraction at 0.1 MPa, 298 K, and equivalence ratios (ϕ) from 0.7 to 1.5 using a spherical constant-volume combustion chamber. The influence of pressure was examined for 20% - 80%DME at 298 K and $\phi = 0.7$ - 1.4 by considering different initial pressures (0.1, 0.3, and 0.5 MPa). A small size reaction mechanism for NH_3/DME/air mixtures was developed and validated against experiments. This mechanism performs well in predicting the laminar burning velocity of NH_3/air, DME/air, and NH_3/DME/air flames as well as the ignition delay time of NH_3, DME, and NH_3/DME oxidation. Detailed kinetic analyses using the mechanism helped us understand the observed effects of DME addition and initial pressure on the laminar burning velocity. The linear increase of laminar burning velocity with increasing DME fraction is mainly attributed to the enhancement of both thermal effect and chemical kinetics effect, while the negative influence of initial pressure is because of the decrease of chemical kinetics effect. In addition, it was found that the main reaction pathways based on N-atom shift with DME addition, whereas those based on C-atom vary little. Furthermore, pressure power exponent β as a function of equivalence ratio shows different behaviors for different DME fractions due to the competition between NH_2 and CH_3 chain-termination reactions for the rich flames. The present work provides experimental measurements of the laminar burning velocity at various conditions and insights into the chemical kinetics for NH_3/DME/air mixtures.

© 2022 The Combustion Institute. Published by Elsevier Inc. All rights reserved.

1. Introduction

Ammonia (NH_3) is a carbon-free fuel and a high hydrogen carrier (17.7wt%) [1]. At present, NH_3 has attracted increasing attention as a potential fuel candidate because of its well-established production, transportation, and storage infrastructure [2]. However, the properties of NH_3 associated with low combustion performance pose significant challenges to its application as a fuel, e.g., high ignition temperature, high latent heat, low boiling point, narrow flammability range, and low laminar burning velocity.

Laminar burning velocity is one of the important combustion properties since it can not only characterize many premixed flame phenomena such as flashback, extinction limits, and flame propagation but also validate chemical kinetics mechanisms [3]. A large number of studies have been conducted on the laminar burning velocity of NH_3/air mixtures [1,2,4–8]. Zakaznov et al. [4] conducted the early experiments of the laminar burning velocity of NH_3/air mixture at atmospheric pressure using the cylindrical-tube method. Hayakawa et al. [1] measured the laminar burning velocity of NH_3/air mixtures at various pressures up to 0.5 MPa for the first time using a constant-volume combustion chamber. They concluded that the flame speed decreases with increasing initial pressure, similar to that of hydrocarbon flames. Lhuillier et al. [8] measured the laminar burning velocity of NH_3/air mixtures at initial temperatures from 298 to 473 K using a similar method. The results show that the laminar burning velocity increases with the increase of initial temperature. Overall, the laminar burning velocities of NH_3/air mixtures are very low compared to other common fuels such as methane (CH_4) [3,9–11], methanol (CH_3OH) [12], ethanol (C_2H_5OH) [12], and hydrogen (H_2) [8,13] etc., especially at high pressures.

In order to improve the combustion performance of NH_3, many other fuels were used to co-fire with NH_3, e.g., CH_4 [3,7,14,15], H_2 [8,16–19], syngas [20,21], and alcohol fuels (CH_3OH and C_2H_5OH)

* Corresponding author at: State Key Laboratory of Fire Science, University of Science and Technology of China, Hefei, Anhui 230027, China.
E-mail address: xiaoh@ustc.edu.cn (H. Xiao).

https://doi.org/10.1016/j.combustflame.2022.112372
0010-2180/© 2022 The Combustion Institute. Published by Elsevier Inc. All rights reserved.

[12]. As summarized in a recent review by Elbaz et al. [22], many most recent studies were focused on ethers fuels, such as dimethyl ether (DME) [23,24], diethyl ether (DEE) [25,26], and dimethoxymethane (DMM) [27]. These dual-fuels perform well in both enhancing the NH_3 reactivity and reducing the NH_3 autoignition resistance [22]. Among them, synthetic oxymethylene ethers (CH_3O-$(CH_2O)_n$-CH_3, OME_n) as sustainable oxygenated fuels have a substantial advantage over other hydrocarbon fuels. For example, OME_n owns higher cetane number and oxygen content than diesel fuel, and enables lower emissions of CO_2 and soot because it contains no C-C bond. DME (OME_0) is the simplest ethers fuel, and maintains a gaseous state at normal temperature and pressure. Its physical properties are similar to those of LPG (liquefied petroleum gas) and can be a promising alternative clean fuel. In particular, DME is miscible with NH_3 and their mixtures can remain stable due to their polarities [28]. Therefore, NH_3/DME blends are considered as a promising alternative fuel. Nevertheless, only a few studies have been devoted to the laminar burning velocity of NH_3/DME/air flames [23,29], although DME was adopted to improve NH_3 autoignition ability and shorten the ignition delay time of NH_3 oxidation [24,28]. In a very recent work, Issayev et al. [23] investigated the combustion performance of NH_3/DME/air flames in a rapid compression machine (RCM) and a constant volume spherical reactor (CVSR). This work contributes a pioneering study of the effect of DME addition on the laminar burning velocity of NH_3 in air. They found that the low-temperature ignition behavior of 40%-50% DME addition in NH_3/DME blends is almost the same as that of neat DME. Also, the laminar burning velocity increases with DME fraction from 18% to 47%, and decreases with pressure from 1 bar to 5 bar. Most recently, Yin et al. [29] studied the laminar burning velocity of NH_3/DME blends with 50% DME addition. This study considers higher temperature than in [23]. They found that the reaction networks of NH_3/DME/air flames at lean and rich sides are similar but the preferred pathways are different, and they also point that DME can effectively increase the laminar burning velocity of NH_3 flames.

In general, developing and validating chemical reaction mechanisms is important for both predicting combustion process and understanding the kinetics. There are numerous studies of the chemical kinetics mechanisms for modeling NH_3 combustion, e.g., those by Han et al. [20], Dagaut et al. [30], Nakamura et al. [31], Otomo et al. [32], Methieu and Petersen [33], Okafor et al. [3], Shrestha et al. [34], Mei et al. [2] and Zhang et al. [35], etc. There are also mechanisms for predicting DME combustion, e.g., the mechanism of Zhao et al. [36] which has been widely used. However, the kinetics of NH_3/DME blends has not been well understood, and there are only a few models available for predicting the NH_3/DME/air laminar burning velocity. Recently, Issayev et al. [23] proposed a kinetic model for the combustion of NH_3/DME blends that contains 176 species and 1418 reactions. Yin et al. [29] also suggested a model based on the mechanism from Dai et al [24]. Yin's model has 193 species and 1669 reactions and gives very similar predictions of laminar burning velocity and ignition delay time to those by Issayev's model. Although these two models performed well in predicting their experimental data of laminar burning velocity of NH_3/DME/air flames, they have not been fully validated against additional measurements of the laminar burning velocity of NH_3/DME/air flames, especially for the full range of DME fraction. In addition, these kinetic mechanisms are large in size and cost significantly more computing resources, although they can sometimes give relatively accurate results. Therefore, it is necessary to develop a small-scale mechanism that can accurately predict the oxidation of NH_3/DME blends.

The pressure power exponents β as a classical parameter that describes the dependence of the laminar burning velocity on pressure were studied in various hydrocarbon fuels. For single-fuel combustion, Goswami et al. [37] derived a relationship between power exponents β and equivalence ratio based on measurements of laminar burning velocity in methane, ethane, propane, and n-pentane flames. This is different from and more reasonable than the linear dependence of power exponents β and equivalence ratio suggested by Metghalchi and Keck [38]. Goswami et al. [39] also found that power exponents β in CH_4/air flames shows a non-monotonic behavior with increasing equivalence ratio. In the work of Wang et al. [40], the power exponents β in $CH_4/O_2/N_2$ flames also show a non-monotonic behavior in the rich flames, and the corresponding equivalence ratio of the minimal β is related to oxygen contents. For dual-fuel combustion, Wang et al. [15] studied the power exponents β as a function of equivalence ratio in NH_3/CH_4/air flames, and found that β varies differently for various CH_4 contents. However, pressure power exponents β in NH_3/DME/air have received little attention.

The objective of this work is to study the unstretched laminar burning velocity of NH_3/DME/air mixtures for the full range of DME fractions and elevated pressures up to 0.5 MPa over a wide range of equivalence ratios using the constant-volume combustion method and kinetic modeling. A detailed kinetics mechanism in relatively small size is developed and validated for NH_3/DME/air mixtures. Reaction pathways and sensitivity analysis are also performed to gain insights into the effects of DME fraction and initial pressure on the laminar burning velocity. The influence of DME fraction on pressure power exponents β is also analyzed in detail.

2. Experiment set-up and processing

The experimental setup used in present work was similar to that used in our prior work [41], and thus will be briefly described here. It consists of a spherical constant-volume combustion chamber, a gas premixing chamber, a pressure recording system, a high-speed schlieren cinematography system, a high-voltage ignition system, and a synchronization controller. A temperature control system was incorporated here and it is composed of a K-type thermocouple, a flexible heating jacket, and a PID controller. The temperature inside the chamber was measured using a K-type thermocouple, and the PID controller was used to regulate the heating jacket to heat the mixture with an accuracy of $\pm$ 2 K.

The experiments were conducted in the 4.2 L spherical combustion chamber with an inner diameter of 200 mm. The volume of the premixing chamber is 12.6 L and a magnetic stirrer was used to ensure a perfectly homogeneous mixture. Two 80 mm diameter quartz optical windows were oppositely mounted. The high-speed schlieren cinematography system, which adopts a linear transmission-type layout, consists of an LED white light source, two focusing lenses (120 mm), a knife edge, a slit, and a high-speed camera. The mixture was ignited by spark electrodes with a diameter of 1.5 mm in the center of the chamber. The propagation of flame was recorded by the high-speed camera operating at 10000 fps. The pressure during flame propagation was measured using a pressure transducer (Kistler 601CAA) and recorded by a memory recorder (HIOKI).

Synthetic air ($21\%O_2/79\%N_2$, purity 99.999%), NH_3 (purity 99.999%), and DME (purity 99.99%) used in this work were from Air Liquide (Kunshan) Gas Technology Co., Ltd. The mixture was prepared according to the Dalton's law of partial pressure. Before each experiment, the pressure in both the combustion and premixing chambers was reduced to 0.1 Torr. The pressure transmitter of GTX30A-BA (accuracy of $\pm$ 0.15% of reading) and GTX60A-BA (accuracy of $\pm$ 0.15% of reading) were used to measure the pressure during the mixture preparation. The fresh mixture was stirred for 30 min in the premixing chamber before being fed into the combustion chamber. A short time delay of 30 s was incorporated into the filling sequence before ignition to guarantee an

Table 1
Experiment conditions.

Initial temperature (T_u) / K	Initial pressure (P_u) /MPa	DME fraction (in fuel)	Equivalence ratio (ϕ)
298	0.1	0–100%	0.7-1.5
298	0.1, 0.3, 0.5	20%, 40%, 60%, 80%	0.7-1.4

Table 2
Chemical kinetics mechanisms considered in this work.

Mechanism	Year	Target reactants	Number of species	Number of reactions
Dagaut-Mech [30]	2008	Oxidation of HCN	41	250
Mathieu-Mech [33]	2015	Oxidation of NH_3 and C1	54	278
Nakamura-Mech [31]	2017	NH_3/air	38	232
Otomo-Mech [32]	2018	NH_3/air and NH_3/H_2/air	32	213
Okafor-Mech [3]	2018	NH_3/CH_4/air	59	356
GRI Mech 3.0 [57]	/	Oxidation of C1-C3	53	325
Shrestha-Mech [34]	2018	NH_3/air and NH_3/H_2/air	125	1090
Mei-Mech [2]	2019	NH_3/O_2	38	265
Han-Mech [20]	2020	$NH_3/CO/H_2$/air	35	177
Zhang-Mech [35]	2021	Oxidation of NH_3/H_2	38	263
Zhao-Mech [36]	2008	DME/air	55	290
Dai-Mech [24]	2021	Oxidation of NH_3/DME	189	1657
Issayev-Mech [23]	2022	NH_3/DME/air	176	1418

Note: C1 and C3 denote the C-containing species.

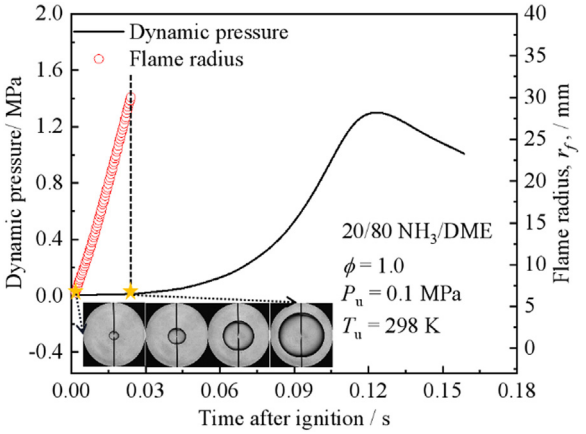

Fig. 1. Time histories of dynamic pressure and flame radius recorded inside the spherical constant-volume bomb, and flame propagation schlieren images during the constant pressure stage.

initially quiescent mixture. Each experiment was repeated at least 3 times to ensure repeatability, and obtain the mean and standard deviation values. The detailed evaluation process of experimental uncertainty was provided in the *Supplementary Material*. Experiments were conducted under various conditions in terms of initial pressure, DME fraction, and equivalence ratio, as summarized in Table 1.

The flame radius, r_f, was evaluated from the schlieren images. The flame radius range, 6 mm < r_f < 30mm, was chosen here to avoid the influences of ignition and wall confinement [42–45]. Figure 1 shows the experimental data extracted in this range. The flame propagation speed, S_b, was calculated from the time derivative of flame radius, $S_b = dr_f/dt$, where t is the time from spark ignition. Spherical flame is a typically stretched flame, and the effect of stretch on flame characteristics must be considered [1]. The stretch rate, κ, i.e., the temporal rate of the change in elementary area of flame front, A, can be expressed by $\kappa = (1/A)/(dA/dt) = (2/r_f)S_b$. A widely used linear method was applied to calculate the stretched flame propagation speed, S_b=$S^0{}_b$–$L_b k$, where $S_b{}^0$ is the unstretched flame propagation speed and can be obtained by extrapolating κ to zero [46]. The quantity L_b is the Markstein length for burned gases. In addition, a nonlinear extrapolation, $(S_b/S_b{}^0)^2\ln(S_b/S_b{}^0)^2 = -2(L_b\kappa/S_b{}^0)$, proposed by Kelley and Law [47], was also tested and it yielded nearly the same results. The comparison in laminar burning velocity of NH_3/DME/air flames between both methods is given in the *Supplementary Material* (see Fig. S4). In this work, we only discuss the results of linear analysis.

Finally, the laminar burning velocity, S_L, can be calculated from the mass conservation across the thin flame front, $S_L = S_b{}^0(\rho_b/\rho_u)$, where ρ_b and ρ_u are the densities of the burned and unburned gases, respectively. These densities were calculated using the Equilibrium module of CHEMKIN-PRO [48].

3. Kinetic modeling

3.1. Model development

The present kinetic mechanism was updated upon the mechanism proposed by Zhao et al. [36]. This mechanism was chosen in this study because it can give predictions of the laminar burning velocity, ignition delay time, and flame species that agree well with the measurements of DME combustion [36]. In addition, it was shown in previous work [49,50] that the mechanism of Zhao et al. [36] is preferable for predicting the laminar burning velocity of DME/air flames. Here, important reactions associated with NH_3 sub-mechanism and C-N sub-mechanism were collected to develop a mechanism for predicting the combustion behavior of NH_3/DME blends. The details of the model development for NH_3/DME/Air in this work are as follows.

NH_3 sub-mechanism: The NH_3 sub-mechanism of present model is selected based on the work of Han et al. [20]. In the work of Han et al. [20], reactions with negligible influence were removed to keep the NH_3 sub-mechanism in a minimal size through reaction sensitivity analyses and path analyses. A small-size NH_3 sub-mechanism with 20 species and 130 reactions in small size was obtained. This model was proven to be capable of satisfactorily predicting flame speed and ignition delay time of NH_3 combustion [20].

C-N sub-mechanism: DME/NO_x interactions are essential to reliably predict the oxidation of NH_3/DME blends [23, 24], because a fraction of NH_3 is oxidized to NO_x during ignition as well as combustion process. Shrestha et al. [51] developed a comprehensive kinetic model for the oxidation of DME and DMM

with the presence of NO_x. They proposed eight crucial cross-reactions between carbon and nitrogen chemistry in accommodating DME/NO_x interactions. These reactions are adopted in present model. In addition, the DME/amine subset is here drawn from recent work of Dai et al. [24]. In this subset, the reaction of DME + NH_2 is the most important step since the NH_2 radical may abstract H-atom from DME to form CH_3OCH_2. The rate constant of $CH_3OCH_3 + NH_2 = CH_3OCH_2 + NH_3$ is calculated from ab initio theory by Dai et al. [24]. The NH_2 radical may recombine with CH_3OCH_2 forming $CH_3OCH_2NH_2$, $CH_3OCH_2 + NH_2(+M) = CH_3OCH_2NH_2(+M)$. Here, the thermodynamic properties of $CH_3OCH_2NH_2$ adduct and the derived radicals are also calculated from the ab initio methods [24]. Other reactions between NH_2 and stable species are also included, e.g., $CH_2O + NH_2$ and $CH_4 + NH_2$, and the rate parameters of $CH_2O + NH_2 = HCO + NH_3$ are given following the theoretical study by Li and Lu [52]. The reaction $CH_3 + NH_2(+M) = CH_3NH_2(+M)$ plays an important role in NH_3 oxidation [29], and the rate coefficients of this reaction are given according to Jodkowski et al. [53]. The CH_3NH_2 subset is extracted from Glarborg et al. [54]. In addition, Wang et al. [12] found that the C-N reactions from a recently updated mechanism by Konnov et al. [55] can well predict the combustion properties of NH_3/hydrocarbon blends. Thus other simple C-N interaction reactions in this work are selected from the Konnov mechanism.

Finally, the kinetic model that consists of 102 species and 594 elementary reactions in relatively small size is developed. The Gas-Phase kinetics, thermodynamic, and transport data files of the present model are given in the *Supplementary Materials*. The thermodynamic and transport data are selected from the corresponding mechanisms. The source of all the reactions mentioned above can be found in the Gas-Phase kinetics file.

Numerical simulations of S_L of NH_3/DME/air flames in this study were performed using the premixed module of CHEMKIN-PRO [48], a one-dimensional freely propagating laminar flame model. Thermal diffusion (Soret effect) and multicomponent transport were taken into consideration in the simulations. For each case in this study, at least 200 grid points were used with CURV 0.05 and CRAD 0.05. In addition to laminar burning velocity, ignition delay time is often used to validate the mechanisms. Therefore, ignition delay time of NH_3 and DME oxidation was also calculated herein with the closed homogeneous module of CHEMKIN-PRO [48] and compared to the experimental results of Mathieu and Petersen [33], Burke et al. [56], and Issavey et al. [23]. For the convenience of discussion, these mechanisms used here were referred to as Name-Mech. For example, the mechanisms by Zhao et al. [36], Han et al. [20], Dagaut et al. [30], Nakamura et al. [31], Otomo et al. [32], Mathieu and Petersen [33], Okafor et al. [3], Shrestha et al. [34], Mei et al. [2], Zhang et al. [35], Issayev et al. [23], and Dai et al. [24] appearing below were called Zhao-Mech, Han-Mech, Dagaut-Mech, Nakamura-Mech, Otomo-Mech, Mathieu-Mech, Okafor-Mech, Shrestha-Mech, Mei-Mech, Zhang-Mech, Issayve-Mech, and Dai-Mech, respectively. The details of these kinetic models were tabulated, as show in Table 2.

3.2. Model validation

Figure 2 shows the measured and simulated laminar burning velocity of (a) NH_3/air and (b) DME/air flames at 0.1 MPa and 298 K as a function of equivalence ratio in comparison to the results reported in literature. For the NH_3/air flames, the experimental results by different researchers in literature all reach the peak value around ϕ = 1.1, as shown in Fig. 2a. All the measurements show a good agreement at lean and stoichiometric burn, while discrepancies of 1-2 cm/s are seen at the rich burn. The experimental data in this study are close to those of Ronney et al. [5] and Mei et al. [2] for the full range of equivalence ratio considered, $0.8 \leq \phi \leq 1.3$. The models considered here can give good predictions of laminar burning velocity for a certain or full range of equivalence ratio, although there are differences between them. For example, present model, Han-Mech, Okafor-Mech, and Otomo-Mech perform well at atmospheric pressure condition considering the experimental uncertainty.

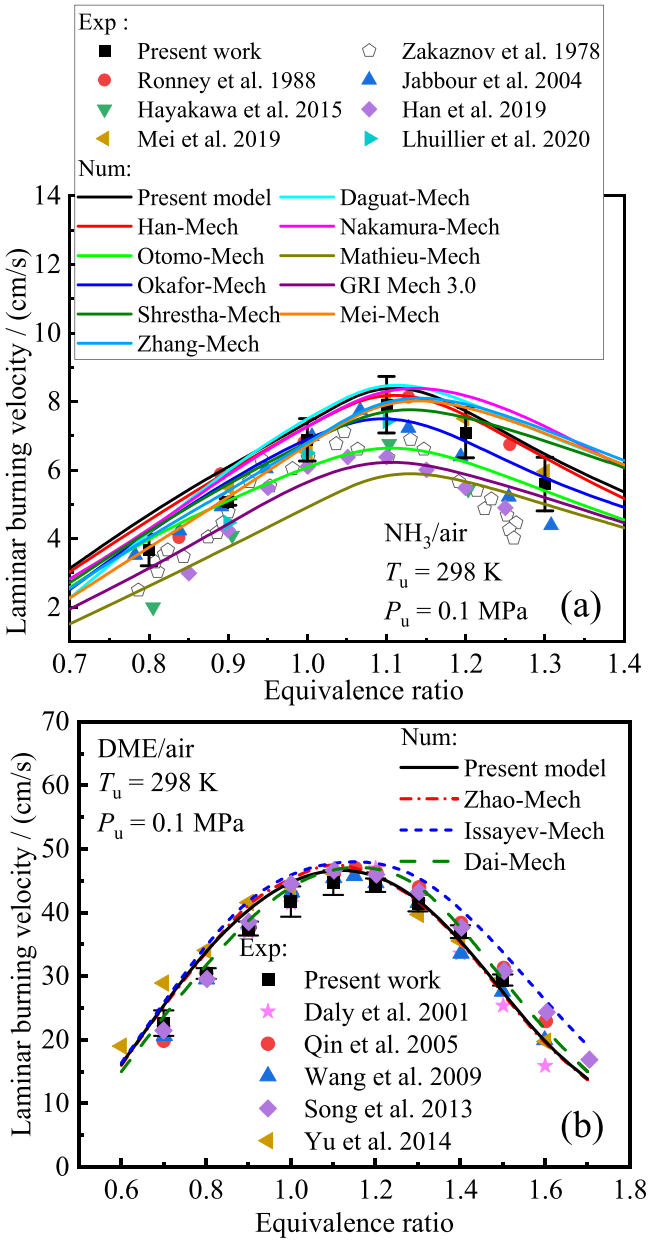

Fig. 2. Laminar burning velocity of (a): NH_3/air and (b): DME/air flames as a function of equivalence ratio at P_u = 0.1 MPa, T_u = 298 K. Symbols: measured results in both this work and literature [1,2,4–8,50,58–61]. Lines: the simulated results of the present model and previous models [2,3,20,23,30–36,57].

For the DME/air flames, the experimental laminar burning velocity shows a good agreement with those in literature, as shown in Fig. 2b. As to simulations, present model slightly over-predicts the current laminar burning velocity of DME/air flames for $\phi \leq 1.2$, while yields results that are very close to the experiments for the rich side (ϕ = 1.4 - 1.5). The predictions of present model agree well with the measurements from Yu et al. [50] for most conditions, except ϕ = 0.6 - 0.7. There are differences between the ex-

periments in literature themselves, and this may due to different uncertainties of different apparatuses in these experiments. Overall, the predictions of present model are in quite reasonable agreement with the experiments. Zhao-Mech gives predictions closely to present model for the full range of equivalence ratio considered. In addition, Issayev-Mech gives similar results to the present model and Zhao-Mech for the lean side and stoichiometric combustion, whereas slightly over-predicts most of the measurements from literature at ϕ = 1.2 - 1.7. However, the predictions of Issayev-Mech basically agree with the measurements from Qin et al. [59] and Song et al. [61] at the rich side. Dai-Mech also predicts well the data in literature, and agrees with present experiments at ϕ = 0.7 - 1.1 and ϕ = 1.4 - 1.5, while slightly over-predicts current measurements at ϕ = 1.2 - 1.3. In brief, all of the four models can give reasonable prediction of the laminar burning velocity of DME/air flames, although there are some differences between them.

Considering the significant uncertainties in the laminar burning velocity of NH_3/air flames, five models were selected from the above NH_3 mechanisms (see Table 2) and compared with the literature data of laminar burning velocity of NH_3/Syngas/air and NH_3/H_2/air flames with 60% NH_3 addition at various equivalence ratios and normal temperature and pressure (T_u = 298 K, P_u = 1.0 atm). The results are shown in Fig. 3. It is shown that Okafor-Mech under-predicts the measurements for both NH_3/Syngas/air and NH_3/H_2/air flames at various equivalence ratios. Shrestha-Mech under-predicts the experiments for both NH_3/Syngas/air and NH_3/H_2/air flames for ϕ < 1.35. Nevertheless, for ϕ > 1.35, this model yields predictions, in good agreement with the measurements of NH_3/Syngas/air flames, but over-predicts the measurements of NH_3/H_2/air flames. Han-Mech gives better prediction for NH_3/Syngas/air flames than for NH_3/H_2/air flames although under-predicts the measured results of the two types of flame at stoichiometric combustion. In addition, present model and Daguat-Mech show similar predictions at ϕ < 1.4, and both of them agree well with the experiments of the two flames at ϕ < 1.2, while over-predict the measurements at ϕ > 1.2. In general, these mechanisms need to be further improved to well predict the experiments of NH_3/Syngas/air or NH_3/H_2/air flames for all conditions.

Figures 4 and 5 show the comparison between predictions of the present model and experimental data in [23,29] of laminar burning velocity for NH_3/DME/Air flames at various equivalence ratios for different initial pressures (0.1 - 0.5 MPa), temperatures (298 - 423 K), and DME fractions (18% - 50%). For normal temperature, the present model agrees well with the measurements at both atmosphere and elevated initial pressures for various equivalence ratios. As the initial temperature increases, the present model reproduces well the experimental data at the rich side, and slightly over-predicts at lean and stoichiometric combustion with deviation less than 8%. Overall, the present model performs well in predicting the laminar burning velocity of NH_3/DME/Air flames.

Figure 6 shows the comparison in ignition delay time between the present model, Issayev-Mech, Dai-Mech, and experiments for NH_3/DME/Air mixtures with 25% - 50%DME addition at 20 - 40bar. The experimental data in Fig. 6 are from Issayev et al. [23]. Issayev-Mech over-predicts the ignition delay time of stoichiometric NH_3/DME/Air mixtures at 25%DME addition, and under-predicts at 50%DME addition. Dai-Mech almost agrees well with the measurements at all conditions considered. Present model gives results in good agreement with the experiments for 40% and 50%DME additions, but over-predicts the experiments for 25%DME addition. The comparison result suggests that the present model may need further improvement in predicting ignition delay time of NH_3/DME blends with low DME fraction. It should be noted that the volume profiles were not considered in this work, and differences in ignition delay time can be expected when taking into account the heat loss in rapid compression machine in simulations [23,24]. This is planned as part of future work.

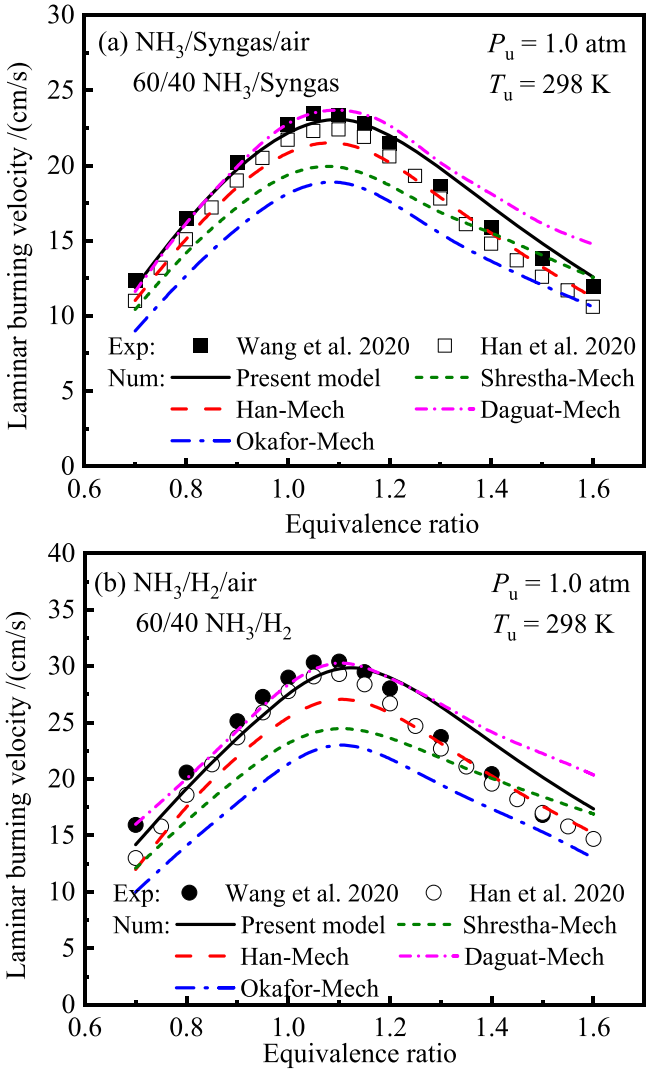

Fig. 3. Laminar burning velocity of (a) NH_3/Syngas/air, (b) NH_3/H_2/air flames as a function of equivalence ratio at T_u = 298 K, P_u = 1 atm. Symbols: experimental data from literature of Wang et al. [62] and Han et al. [20]. Lines: the simulated results of the present model and previous models [14,20,30,34].

Additional comparisons of laminar burning velocity and ignition delay time between the present model and the experiments from literature are given in the *Supplementary Material* (see Figs. S1-S3 and S5-S6). The kinetic model developed by Yin et al. [29] was not tested in this work since the predictions of this model are very similar to those of Issayev-Mech, as shown in [29].

Overall, the present model can well predict the laminar burning velocity of NH_3/air, DME/air, and NH_3/DME/air flames as well as the ignition delay time of oxidation of NH_3, DME, and NH_3/DME. Therefore, this model was used in this study to analyze the NH_3/DME/air laminar flames and oxidation processes, and it does quite well for NH_3/DME/air mixtures at various conditions, as will be shown below.

4. Results

Figure 7 shows the measured and simulated laminar burning velocity of NH_3/DME/air flames as a function of equivalence ratio at 0.1 MPa and 298 K for various NH_3/DME blends. It can be seen that the experimental data reach the peak value at about ϕ = 1.1

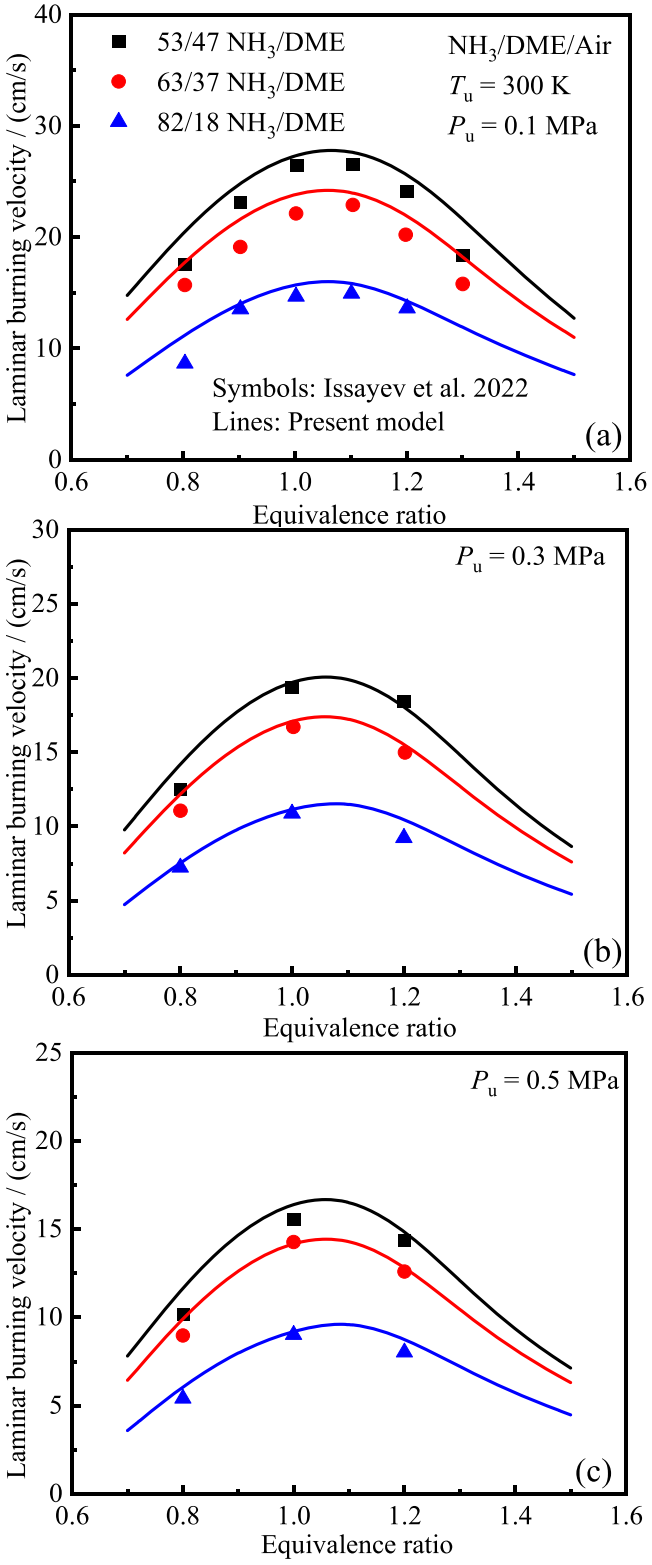

Fig. 4. Laminar burning velocity of NH_3/DME/air flames as a function of equivalence ratio at T_u = 300 K, P_u = 0.1, 0.3, 0.5 MPa. Symbols: experimental data from literature of Issayev et al. [23]. Lines: present model.

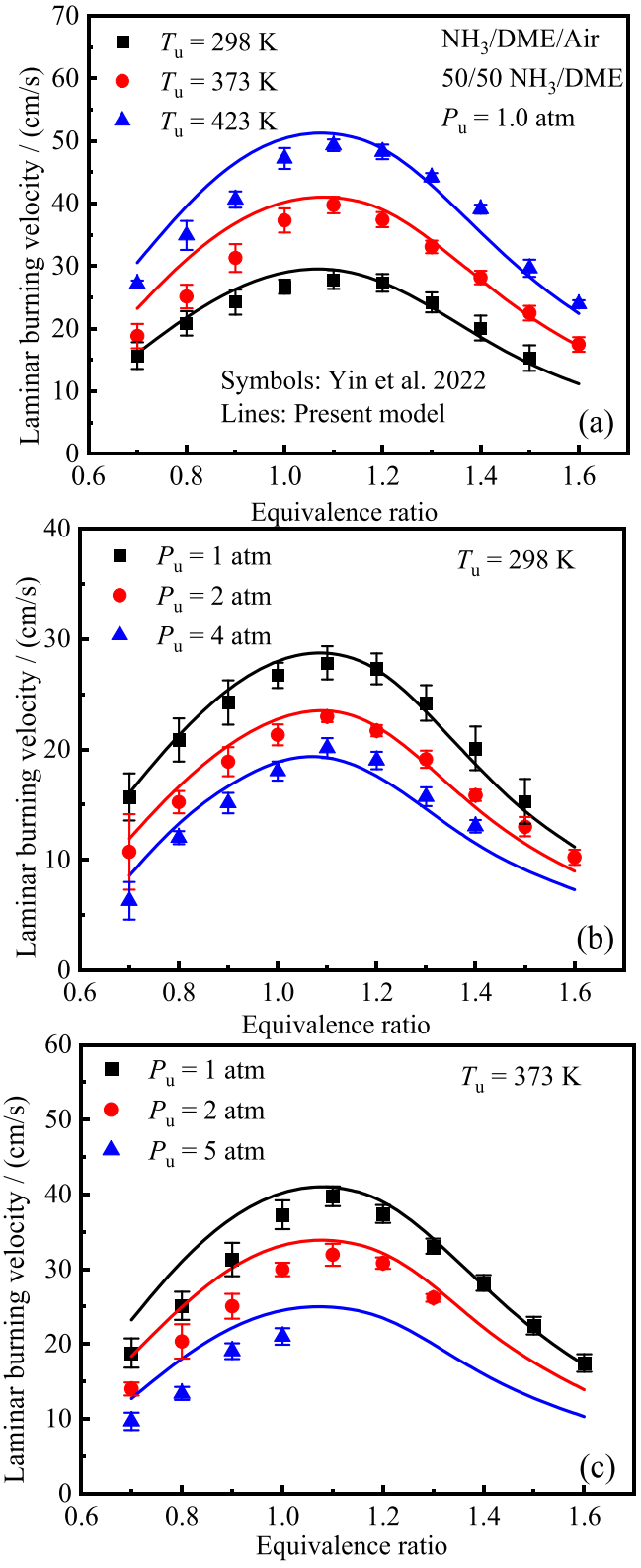

Fig. 5. Laminar burning velocity of NH_3/DME/air flame with 50%DME addition as a function of equivalence ratio at T_u = 298, 373 K, 423 K, P_u = 0.1, 0.3, 0.5 MPa. Symbols: experimental data from literature of Yin et al. [29]. Lines: present model.

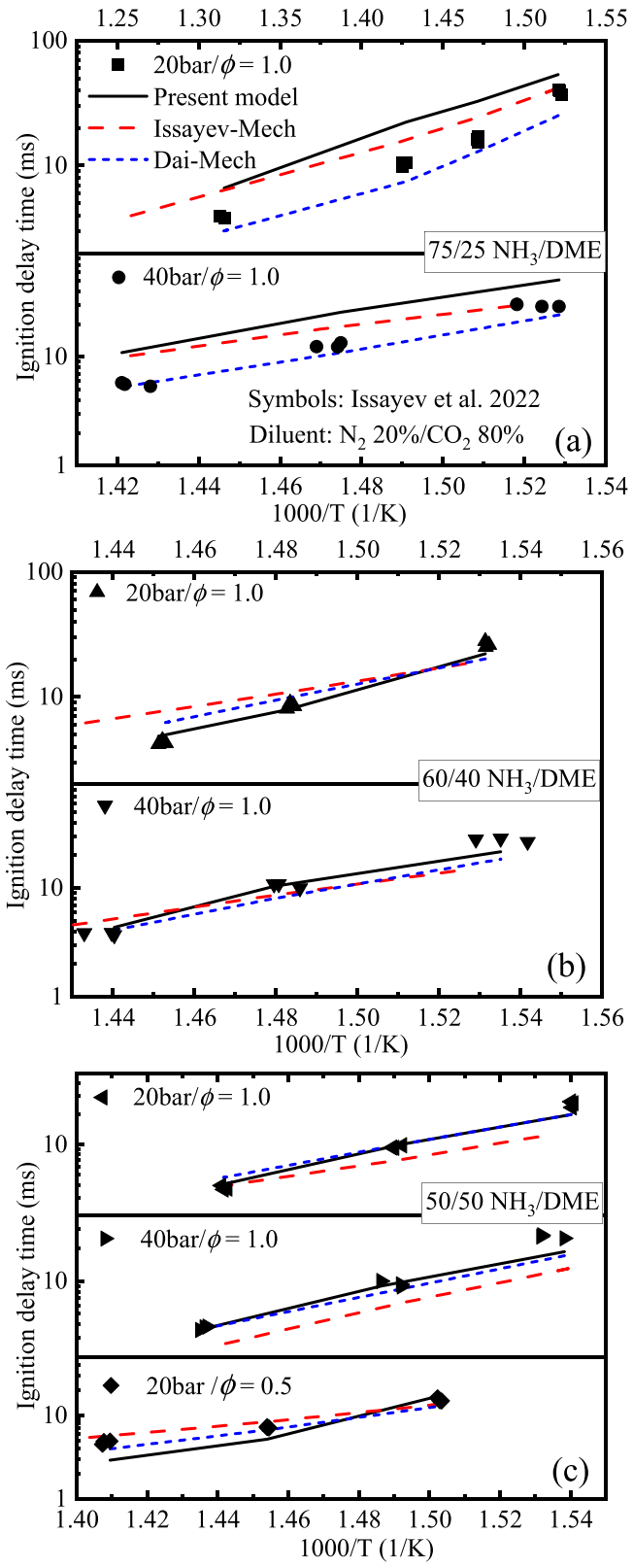

Fig. 6. Ignition delay time of NH_3/DME oxidation at specified conditions. Symbols: experimental data from literature of Issayev et al. [23]. Solid lines: Present model. Long dashed lines: Issayev-Mech. Short dashed lines: Dai-Mech.

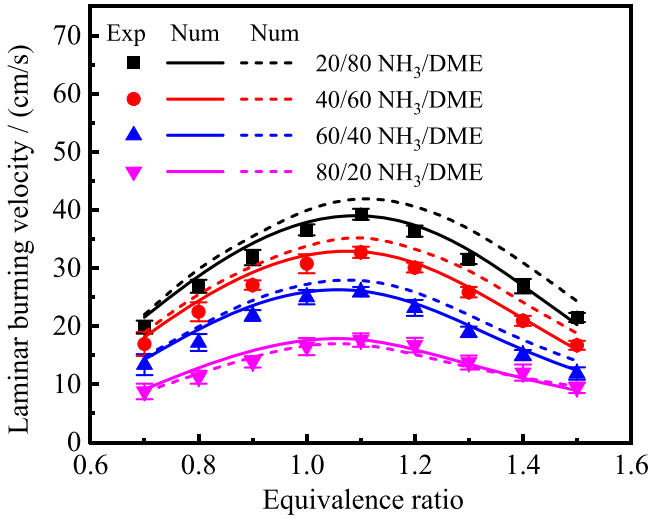

Fig. 7. Laminar burning velocity of NH_3/DME/air flames as a function of equivalence ratio at P_u = 0.1 MPa, T_u = 298 K. Symbols: measurements in this study. Solid Line: present model. Dashed line: Issayev-Mech.

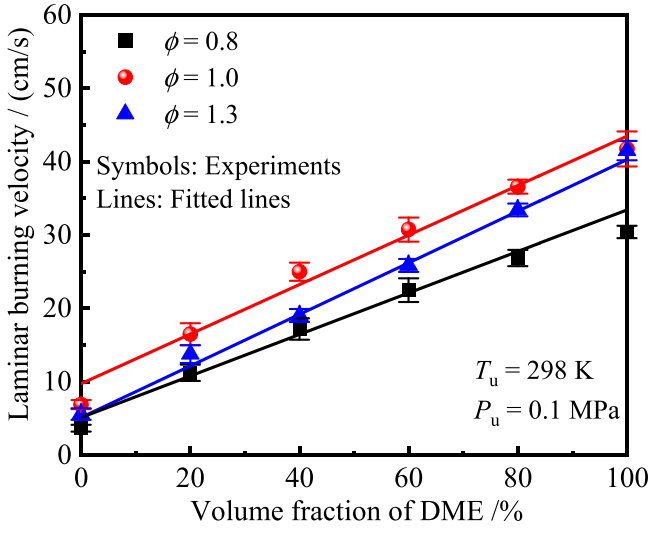

Fig. 8. Laminar burning velocity of NH_3/DME/air as a function of DME fraction at T_u = 298 K, P_u = 0.1 MPa and the equivalence ratio of ϕ = 0.8, 1.0, and 1.3. Symbols: measurements in this work. Lines: Fitted lines.

for different DME fractions. The maximum value increases from 17.61 cm/s (20%DME) to 39.25 cm/s (80%DME). This indicates that increasing DME fraction greatly promotes the laminar flame propagation of the mixture. Figure 8 shows the measured and fitted laminar burning velocity of NH_3/DME/air as a function of DME fraction at 0.1 MPa, 298 K and the equivalence ratio of ϕ = 0.8, 1.0, and 1.3. It should be noted that the increase of the laminar burning velocity is linear when increasing DME fraction. Compared with the measurements, the present model gives good predictions, although there are slight differences at ϕ = 0.8 - 1.0 for various DME fractions (20%DME - 80%DME). Issayev-Mech gives results that agree well with the current experiments for 20%DME addition, whereas over-predicts the measurements for 40%DME - 80%DME addition at the rich side. In addition, the discrepancies between experiments and predictions by Issayev-Mech become larger as DME fraction increases, as shown in Fig. 7. This indicates that the present model performs better for the NH_3/DME/air flames at normal temperature and pressure (298 K and 0.1 MPa).

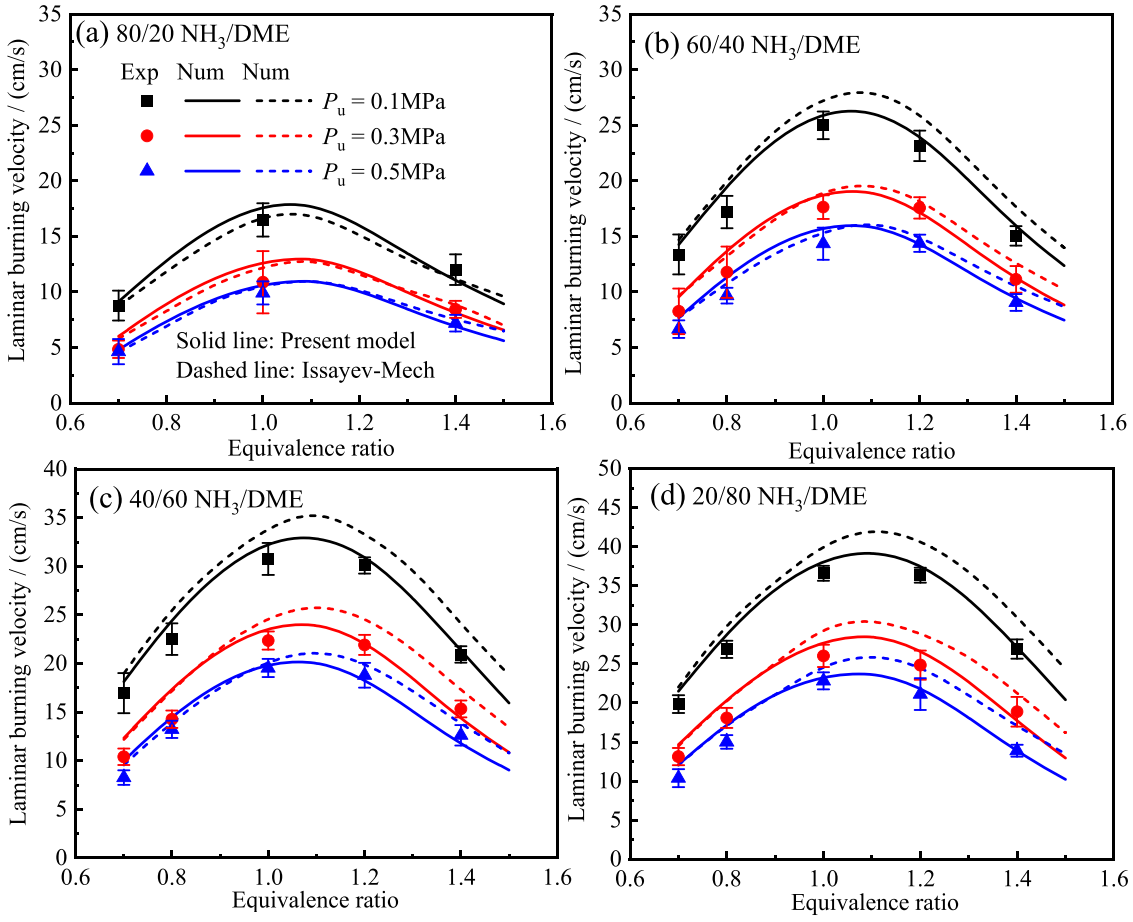

Fig. 9. Measured and simulated laminar burning velocity of NH_3/DME/air flames as a function of equivalence ratio at T_u = 298 K and P_u = 0.1, 0.3, and 0.5 MPa for various DME fractions.

Figure 9 shows the measured and simulated laminar burning velocity of NH_3/DME/air flames as a function of equivalence ratio at T_u = 298 K, and P_u = 0.1, 0.3, and 0.5 MPa for various DME fractions: (a) 20%, (b) 40%, (c) 60%, and (d) 80%. Figure 10 shows the laminar burning velocity of NH_3/DME/air as a function of initial pressure at T_u = 298 K and various equivalence ratios. For different initial pressures, the laminar burning velocity shows a similar tendency with increasing equivalence ratio, and peaks around ϕ = 1.1, as shown in Fig. 9. For a fixed equivalence ratio, increasing initial pressure decreases the laminar burning velocity, and the drop rate becomes smaller as the pressure increases, as shown in Fig. 10. As to simulations, the present model and Issayev-Mech give similar results for the lean side. Nevertheless, there are discrepancies between them for the rich side, as shown in Fig. 9. In general, the results given by present model are in satisfactory agreement with the experimental measurements for NH_3/DME/air mixtures at different conditions even at high initial pressures considered, although minor differences can be seen for lean conditions.

In general, the dependence of laminar burning velocity on initial pressure can be expressed as $S_L/S_{L0}=(P/P_0)^{\beta}$, where S_{L0} is the laminar burning velocity at pressure P_0, and β is the pressure power exponent. For most fuels, laminar burning velocity decreases with increasing initial pressure, and thus $\beta < 0$. The pressure power exponent β can be related to the overall reaction order, $\beta = n/2\text{-}1$ [63]. The reaction order is considered to be closely connected with chain branching-termination reactions [63]. Therefore, the effect of pressure on flame speed can be explained through chain mechanism. For instance, the overall reaction order n should be close to 2 when a flame is dominated by two-body reactions. Three-body termination reactions, e.g., H + O_2 (+ M) = HO_2 (+ M), generally play a negative role and tend to reduce n, leading to $n < 2$ and $\beta < 0$. The measured and predicted results of β in this work are displayed in Fig. 11. Here β is extracted using a least-square fit to the empirical correlation, $S_L/S_{L0}=(P/P_0)^{\beta}$, where P is in the range of 0.1 MPa - 0.5 MPa. Therefore, β is a function of laminar burning velocity, $S_L^{P_i}$, i.e., $\beta = f(S_L^{P_1}, S_L^{P_2}, ..., S_L^{P_m})$. The uncertainties of β at different conditions are thus associated with the accuracy of the laminar burning velocity, and can be calculated using the error propagation formula [37],

$$\Delta\beta = \left(\sum_i \left[\left(\ln\frac{P_i}{P_0} - \overline{\ln\frac{P_i}{P_0}}\right)\cdot\frac{\Delta S_L^{P_i}}{S_L^{P_i}}\right]^2\right)^{0.5} \Big/ \left(\sum_i \ln^2\frac{P_i}{P_0} - m\cdot\left(\overline{\ln\frac{P_i}{P_0}}\right)^2\right) \quad (1)$$

where m = 3 is the number of data points, $\Delta S_L^{P_i}$ is the uncertainty of the laminar burning velocity at initial pressure P_i, $\overline{\ln(P_i/P_0)} = (\sum_i \ln(P_i/P_0))/m$ is the mean logarithmic normalized pressure, and P_0 = 0.1 MPa is the reference pressure. The uncertainties of β for various DME fractions at different equivalence ratios are listed in Table 3.

Figure 11 shows the measured and predicted pressure power exponent β of NH_3/DME/air flames with various DME fractions as a function of equivalence ratio, in comparison to the prediction by the Issayev-Mech. The predictions of both mechanisms agree well with the experiments at a wide range of equivalence ratio for all DME fractions considering the experimental uncertainties, although there are differences between them. Figure 11a

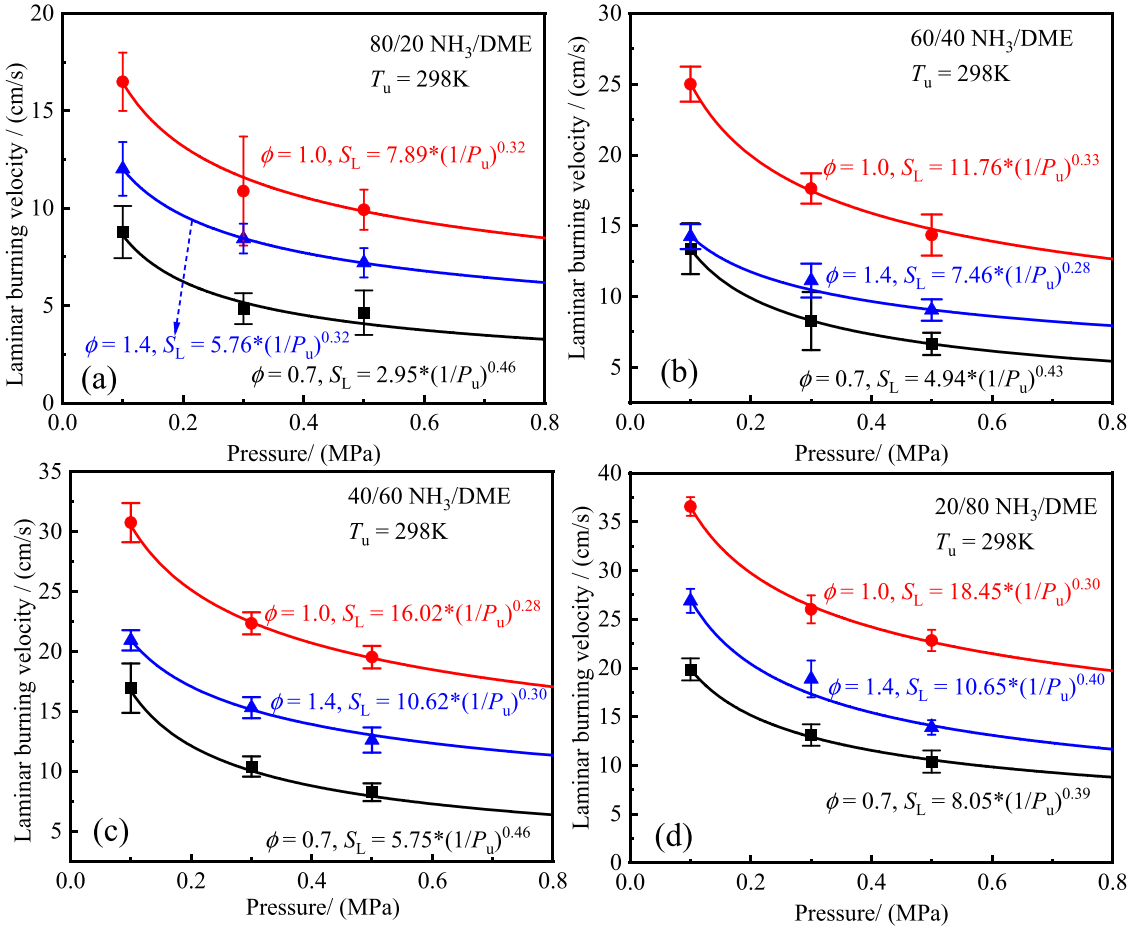

Fig. 10. Laminar burning velocity of NH_3/DME/air as a function of initial pressure at T_u = 298 K and the equivalence ratio of ϕ = 0.7, 1.0, and 1.4 for various DME fractions. Symbols: measurements in this work. Lines: fitted curves.

Table 3
The pressure power exponents with experimental uncertainties for NH_3/DME/air flames at various DME fractions.

DME fractions	ϕ = 0.7	ϕ = 0.8	ϕ = 1.0	ϕ = 1.2	ϕ = 1.4
20%	-0.419 ± 0.165	/	-0.326 ± 0.089	/	-0.319 ± 0.095
40%	-0.434 ± 0.115	-0.355 ± 0.074	-0.341 ± 0.063	-0.288 ± 0.049	-0.309 ± 0.060
60%	-0.446 ± 0.095	-0.343 ± 0.060	-0.283 ± 0.044	-0.292 ± 0.037	-0.310 ± 0.052
80%	-0.399 ± 0.076	-0.361 ± 0.043	-0.296 ± 0.032	-0.339 ± 0.054	-0.397 ± 0.041

shows that, for 20%DME fraction, β increases monotonously with increasing equivalence ratio, and the growth rate decreases when ϕ >1.0. As DME fraction increases (>~40%), as shown in Fig. 11(b-c), the variation of β with increasing equivalence ratio shows a non-monotonic behavior: first, it increases with increasing equivalence ratio, reaching a peak value around ϕ =1.0, then decreases with equivalence ratio, reaching a minimal value around ϕ =1.4, and finally increases again. The corresponding equivalence ratio of these minimal values slightly increases with increasing DME fraction, from ϕ = 1.33 for 40%DME to ϕ = 1.47 for 80%DME. The different behaviors of β for various DME fractions implies that NH_3 chemistry dominates the laminar burning velocity for DME fraction less than 40%, whereas DME chemistry becomes dominant when DME fraction is higher than 40%.

The values of β are very close for various DME fractions at a fixed equivalence ratio when ϕ ≤1.0. This indicates that the quantitative effect of pressure on laminar burning velocity of NH_3/DME/air flames with various DME fractions is similar at lean-fuel and stoichiometric combustion. The peak value appearing around ϕ = 1.0 means that the pressure has a more significant negative influence on the laminar burning velocity at lean-fuel than stoichiometric condition. In addition, the value of β on rich side decreases with the increase of DME fraction due to the appearance of non-monotonic behavior. This means that increasing pressure has a greater influence on the laminar burning velocity for high DME fraction flames (>~40%) at rich side, especially around ϕ = 1.4. In addition, non-monotonic dependence of β on ϕ was found for pure hydrocarbon fuels [15, 39, 40]. Therefore, the monotonic trend of β in high NH_3 content may be attributed to the influence of NH_2 for rich-fuel condition, and as will be discussed in Section 5.2.

5. Discussion

5.1. Effect of DME fraction

Figure 12 shows the major reaction pathways of different NH_3/DME/air flames based on N-atom (0%DME, 20%DME and 60%DME) and C-atom (20%DME and 60%DME,100%DME) at 0.1 MPa, 298 K, and ϕ = 1.0. For the pathways of N-atom, NH_3 is

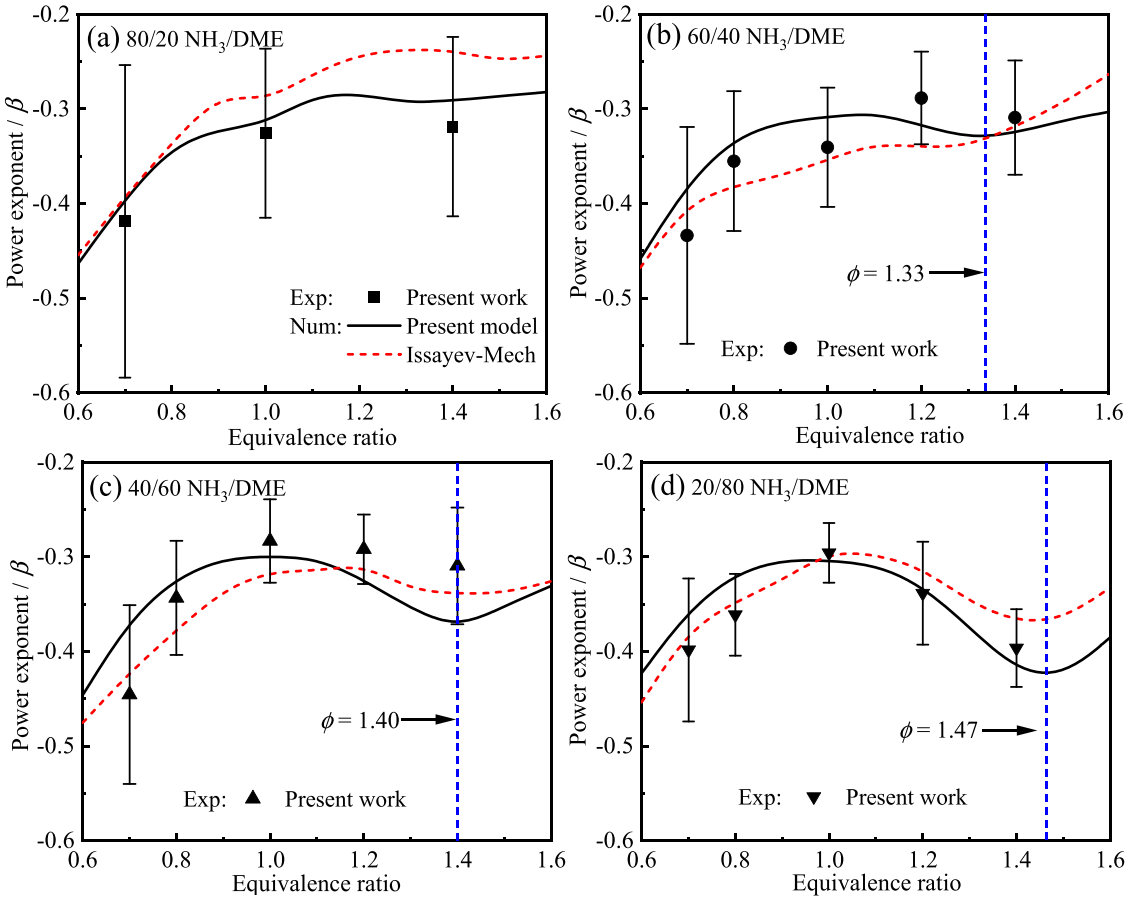

Fig. 11. The pressure power exponent β of NH_3/DME/air flames with various DME fractions as a function of equivalence ratio.

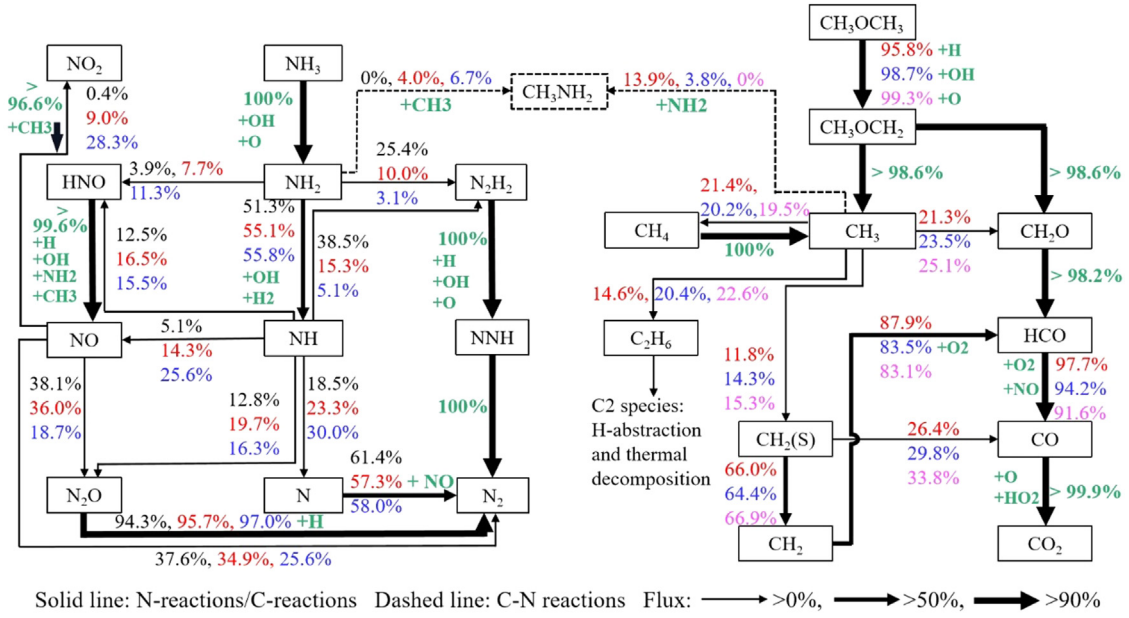

Fig. 12. Reaction pathways analysis for different NH_3/DME/air flames at P_u = 0.1 MPa, T_u = 298 K, and ϕ = 1.0 based on N-atom and C-atom. The four colors mean: black, 0%DME; red, 20%DME; blue, 60%DME; pink, 100%DME; green, the same value for all DME fractions.

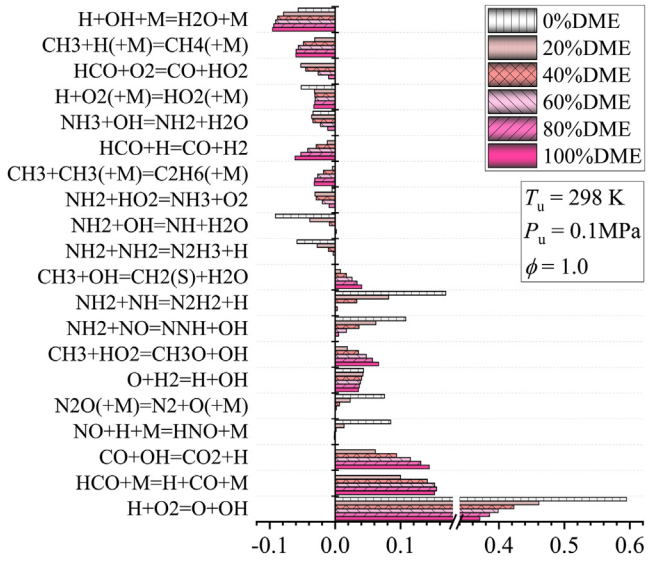

Fig. 13. Sensitivity analysis for laminar burning velocity of NH_3/DME/air flames at P_u = 0.1 MPa, T_u = 298 K, and ϕ = 1.0 for various DME fractions.

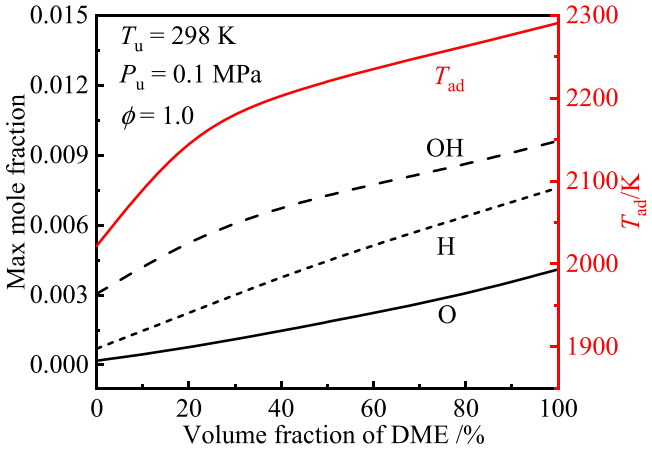

Fig. 14. Simulated adiabatic flame temperature and maximum mole fractions of O, H, and OH of NH_3/DME/air flames as a function of DME fraction at P_u = 0.1 MPa, T_u = 298 K, and ϕ = 1.0.

almost completely consumed by OH and O to form NH_2. Then, NH_2 is mainly oxidized into NH, HNO, and N_2H_2. Among these three species, NH is an indispensable radical in the conversion of NH_3 to N_2 since it involves most of the chain branching reactions. The NH_3 oxidation can be divided into three reaction routes:

(1) NH_3-NH_2-NH-N-N_2;
(2) NH_3-NH_2-(NH-HNO)/HNO-NO-(N_2)/N_2O-N_2;
(3) NH_3-NH_2-(NH-N_2H_2)/N_2H_2-NNH-N_2.

The integrated rate of species production for the key reaction steps ($NH_2 \rightarrow$ NH, $NH_2 \rightarrow$ HNO, and $NH_2 \rightarrow N_2H_2$) in the three routes shows that $NH_2 \rightarrow$ NH has the largest rate of species production, as shown in Fig. 12. This means that route (1) is the major reaction pathway. The integrated rate of species production for the key reaction step in route (3), $NH_2 \rightarrow N_2H_2$, decreases with the increase of DME fraction from 25.4% for 0%DME to 3.1% for 60%DME. By contrast, the integrated rate for key reaction steps in route (1), $NH_2 \rightarrow$ NH, and in route (2), $NH_2 \rightarrow$ HNO, increase from 51.3% to 55.8%, and 3.9% to 11.3%, respectively. This means that the main reaction pathways of NH_3/DME/air flames shift with DME fraction. That is, route (2) becomes more significant than (3) as DME fraction increases.

For pathways based on C-atom, CH_3OCH_3 is also fully consumed through the H abstraction by free radicals (H, OH, and O) to form CH_3OCH_2. CH_3OCH_2 is then oxidized into two major radicals (CH_3 and CH_2O). Thus the CH_3OCH_3 oxidation can be divided into two main reaction routes:

(1) CH_3OCH_3-CH_3OCH_2-(CH_3-CH_2O)/CH_2O-HCO-CO-CO_2;
(2) CH_3OCH_3-CH_3OCH_2-CH_3-CH_2(S)-(CO-CO_2)/CH_2-HCO-CO-CO_2.

The integrated rate of species production shows that route (1) plays a more significant role than route (2) in converting CH_3OCH_3 into CO_2. Comparing the integrated rates of species production between different DME fractions shows that the reaction pathways based on C-atom vary little. In addition, the integrated rate for the formation of C_2H_6, i.e., reaction $CH_3+CH_3(+M) = C_2H_6(+M)$, increases from 14.6% for 20%DME to 22.6% for 100%DME. This means that the higher DME fraction is, the more hydrocarbon intermediates (C_2 species) are generated. There is a cross-reaction between C and N families, $CH_3 + NH_2(+M) = CH_3NH_2(+M)$, which plays a significant role for the combustion of NH_3/DME/air blends. As shown in Figure 12, the integrated conversion rate of NH_2 to CH_3NH_2 increases from 0% for 0%DME to 6.7% for 60%DME, while that of CH_3 to CH_3NH_2 decreases from 13.9% for 20%DME to 0% for 100%DME. This indicates that a higher DME fraction may be more beneficial for the oxidation of N family than C family in the C-N interactions. It also confirms that DME addition can improve the reactivity of NH_3 through C-N interactions, although the contribution is minor. Furthermore, the other C-N interactions, i.e., $CH_3 + HNO = NO + CH_4$ and $CH_3 + NO_2 = CH_3O + NO$, can slightly increase the NO production. This observation is consistent with the result of Meng et al. [64]. The reaction $HCO + NO = HNO + CO$ further promotes the formation of HNO and CO radicals. This suggests that the emissions of NO, NO_2, and CO may influence each other by C-N interactions.

The above results suggest that the variation of DME fraction in NH_3/DME/air blends has a more important influence on the NH_3 reaction pathways than on the DME reaction pathways. Meanwhile, the C-N interactions slightly influence the flame structure and the emissions of NO_x and CO.

Figure 13 shows the sensitivity analysis of the dominant reactions for NH_3/DME/air flames at 0.1 MPa, 298 K, and ϕ = 1.0 with various DME fractions. The chain branching reaction $H + O_2 = O + OH$ has the highest sensitivity for all NH_3/DME/air flames, and its sensitivity decreases as the DME fraction increases. Other high-sensitive reactions, i.e., $HCO + M = H + CO + M$ and $CO + OH = CO_2 + H$, show an increasing sensitivity trend with increasing DME fraction, especially for the reactions with DME fraction less than 40%. In addition, CH_3, as a key radical of DME oxidation, involves many important reactions influencing the laminar burning velocity. For example, the reactions with positive sensitivity coefficients, $CH_3 + HO_2 = CH_3O + OH$ and $CH_3 + OH = CH_2(S) + H_2O$, are significant forward steps in reaction pathway routes (1) and (2) based on C-atom, respectively. The reactions with negative sensitivity coefficients, $CH_3 + H(+M) = CH_4(+M)$ and $CH_3 + CH_3(+M) = C_2H_6(+M)$, are important rate-limiting reactions from DME chemistry in NH_3/DME/air flames. HCO, as another key radical of DME oxidation, participates in the reactions with both positive and negative sensitivity coefficients, i.e., $HCO + M = H + CO + M$, $HCO + O_2 = CO + HO_2$, and $HCO + H = CO + H_2$. Although all the three reactions produce CO, the reaction $HCO + M = H + CO + M$ has a positive effect on the laminar burning velocity, opposite to the other two reactions.

The sensitivity of the NH_3 chemistry reactions decreases rapidly as DME fraction increases, especially these following reactions, $NH_2 + NH = N_2H_2 + H$, $NH_2 + NO = NNH + OH$,

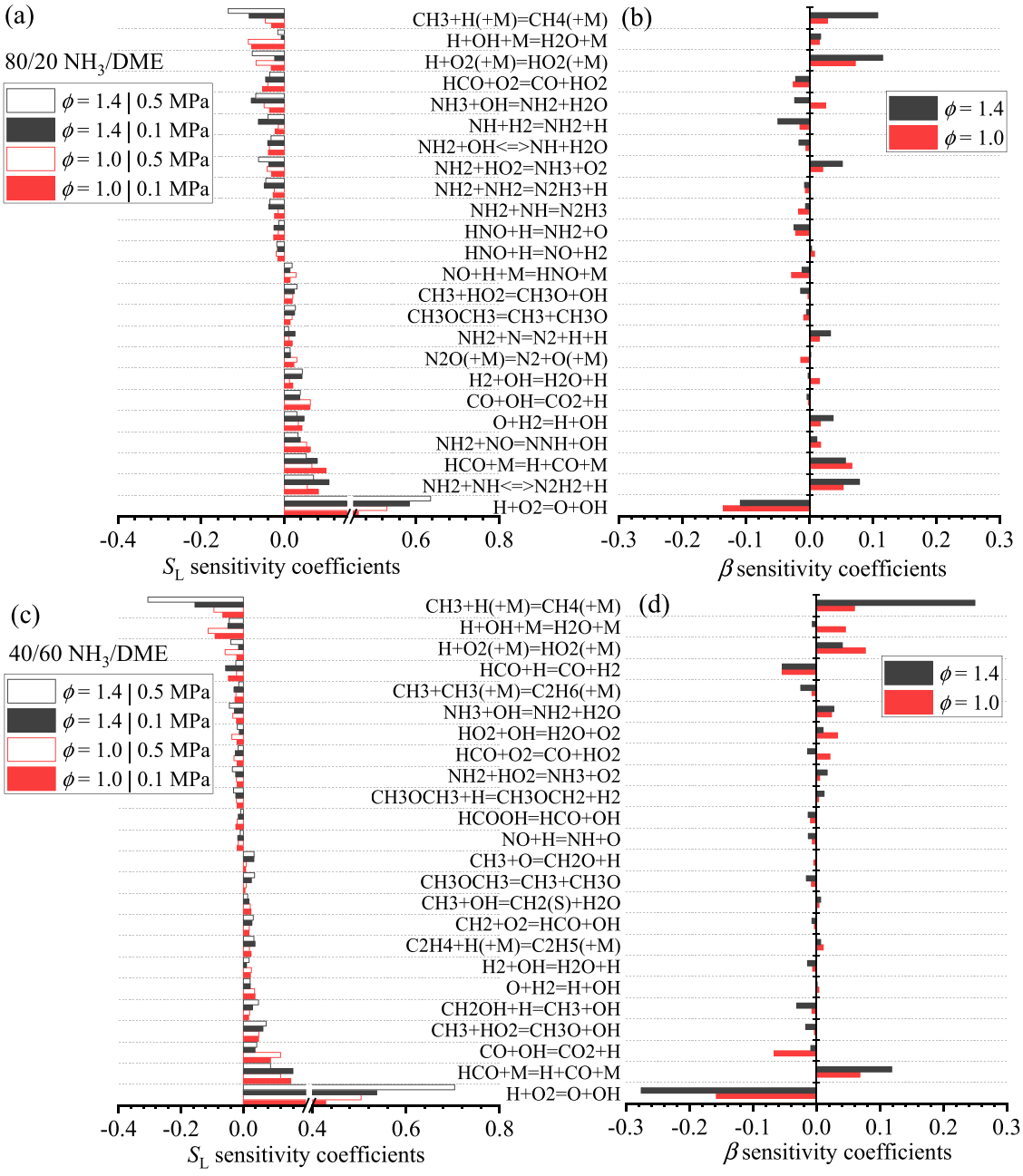

Fig. 15. Sensitivity analysis for laminar burning velocity and pressure exponent (β) of NH_3/DME/air flames with 20% (a-b) and 60%DME (c-d) addition at P_u = 0.1 and 0.5 MPa.

$N_2O(+M) = N_2 + O(+M)$, and $NO + H + M = HNO + M$. The sensitivity coefficients of these reactions with DME fraction higher than 40% can almost be neglected, which confirms that the DME chemistry will dominate the laminar burning velocity of NH_3/DME/air flames for high DME fraction (>~40%). In addition, there are no C-N interactions in the most sensitive reactions, as shown in Fig. 11. This indicates that the interactions between C and N containing species play an insignificant role in predicting the laminar burning velocity of NH_3/DME/air flames. Therefore, NH_3 chemistry and DME chemistry indirectly affect each other by sharing the same OH, H, and O radical pools. Similar findings appear in the oxidation of NH_3/CH_4 blends [3], NH_3/syngas blends [20], and NH_3/DMM blends [27], etc.

The above sensitivity analysis indicates that the reactions with positive sensitivity coefficients produce many free radicals, especially H, OH, and O, and thus promote the reactivity and the laminar burning velocity of NH_3/DME/air flames. On the contrary, the reactions with negative sensitivity coefficient consume these free radicals and thus retard the reactivity.

Figure 14 shows the simulated adiabatic flame temperature (T_{ad}) and maximum mole fractions of O, H, and OH of NH_3/DME/air flames as a function of DME fraction at 0.1 MPa, 298 K, and ϕ = 1.0. The result shows that the maximum mole fractions of O, H, and OH increase with the increase of DME fraction, and it means the enhancement of chemical kinetics effect. This corresponds to the increase of laminar burning velocity with increasing DME fraction. In addition, T_{ad} is greatly elevated with increasing DME fraction, that is, T_{ad} increases from 2021 K for 0%DME (pure NH_3/air) to 2290 K for 100%DME (pure DME/air) flame. As reported in [2], T_{ad} represents the thermal effect on laminar burning ve-

locity. Therefore, as DME fraction increases, the enhanced thermal effect associated with the elevated T_{ad} facilitates the increase of laminar burning velocity.

5.2. Effect of pressure

The increase in initial pressure has a negative effect on the laminar burning velocity (see Fig. 10). Figure 15 shows the sensitivity analysis of the laminar burning velocity of NH_3/DME/air flames with 20% (a) and 60%DME (c) addition for stoichiometric and rich combustion at P_u = 0.1 and 0.5 MPa. For the two DME fractions, H + O_2 = O + OH and HCO + M = H + CO + M are the most sensitive reactions with positive coefficients, while the top sensitive reactions with negative coefficients are CH_3 + H (+ M) = CH_4 (+ M), H + OH +M = H_2O + M, and H + O_2 (+ M) = HO_2 (+ M). These top sensitive reactions dominating the high-temperature oxidation of NH_3/DME are mainly H_2/CO chemistries. The three-body termination reactions of CH_3 to CH_4 is also very important, especially at rich-fuel, even for high ammonia content. These reactions are almost the same as the oxidation of NH_3/CH_4, as detailed by Wang et al. [15].

For low DME fraction, NH_2, NH, NO, and HNO radicals play an important role in affecting flame speeds, as shown in Fig. 15a. It was found that the sensitivities of most of the reactions associated with NH_2 weaken with increasing initial pressure at stoichiometric combustion and rich-fuel. These reactions are NH + H_2 = NH_2 + H, NH_2 + OH = NH + H_2O, NH_2 + NH_2 = N_2H_3 + H, NH_2 + NH = N_2H_3, HNO +H = NH_2 + O, NH_2 + N = N_2 + H + H, NH_2 + NO = NNH + OH, and NH_2 + NH = N_2H_2 + H. In addition, the sensitivity of NH_3 + OH = NH_2 + H_2O is enhanced with increasing pressure at stoichiometric combustion, while weakened at rich-fuel.

For high DME fraction, as shown in Fig. 15c, the reactions associated with CH_3, HCO, CH_2OH, and C_2H_i radicals significantly influence the flame speed. The sensitivities of most of these reactions enhance as pressure increases, except CH_3 + OH = CH_2 (S) + H_2O, C_2H_i reactions (CH_3 +CH_3 (+M) = C_2H_6 (+M) and C_2H_4 + H (+M) = C_2H_5 (+M)), and two HCO reactions (HCO + H = CO + H_2 and HCO + M = H +CO + M). For both low and high DME fractions, the sensitivities of most reactions are stronger in rich-fuel than those in stoichiometric combustion, while the top sensitive three-body termination reaction H + OH + M = H_2O + M with negative coefficient shows importance at stoichiometric combustion.

Similar to the laminar burning velocity sensitivity analysis, the sensitivity coefficients of β can be defined as [37],

$$Sens(\beta, k) = \frac{Sens(S_L, k) - Sens(S_{L_0}, k)}{\beta \ln(P/P_0)}, \quad (2)$$

where S_L and S_{L_0} are the laminar burning velocity at P = 0.5 MPa and P_0 = 0.1 MPa, respectively, and K is the rate constant. Figure 15 also shows the β sensitivity analysis of NH_3/DME/air flames for 20% (b) and 60% (d) DME fraction at ϕ = 1.0 and 1.4, respectively. Comparing the sensitivity between laminar burning velocity and β suggests that the reactions that has an important effect on laminar burning velocity do actually not affect the calculated β coefficients, e.g., NH_2 + NH_2 = N_2H_3 + H and CO + OH = CO_2 + H for 20%DME fraction, and CH_2 + O_2 = HCO + OH, CH_3 + OH = CH_2 (S) +H_2O, and CH_3 + O = CH_2O + H for 60%DME fraction. Therefore, variation in the rate constants of these reactions will have a significant influence on the calculated laminar burning velocity, but has minor effect on calculated pressure exponents β. By contrast, β of some reactions are more sensitive to pressure than laminar burning velocity, especially for low DME fraction, such as NH_2 + NH = N_2H_2 + H, NH_2 + N = N_2 + H + H, NO + H + M = HNO + M, HNO + H = NH_2 + O, NH_2 + HO_2 = NH_3 + O_2, and NH + H_2 = NH_2 + H. In addition, β of these reactions, except NH_2 + N = N_2 + H + H, are more sensitive at rich-fuel than stoichiometric combustion. This indicates that the laminar burning velocity of high-pressure ammonia flame is more difficult to accurately predict than that of high-pressure DME flame, especially for rich-fuel, because of the high sensitivity of β to pressure. Thus β may be regarded as a target for model validation and improvement. Previous works [15,37] related to CH_4, C_2H_6, and C_3H_8 also show discrepancies in sensitivity between laminar burning velocity sensitivity and pressure exponent β for the same reactions. This is consistent with the observation here.

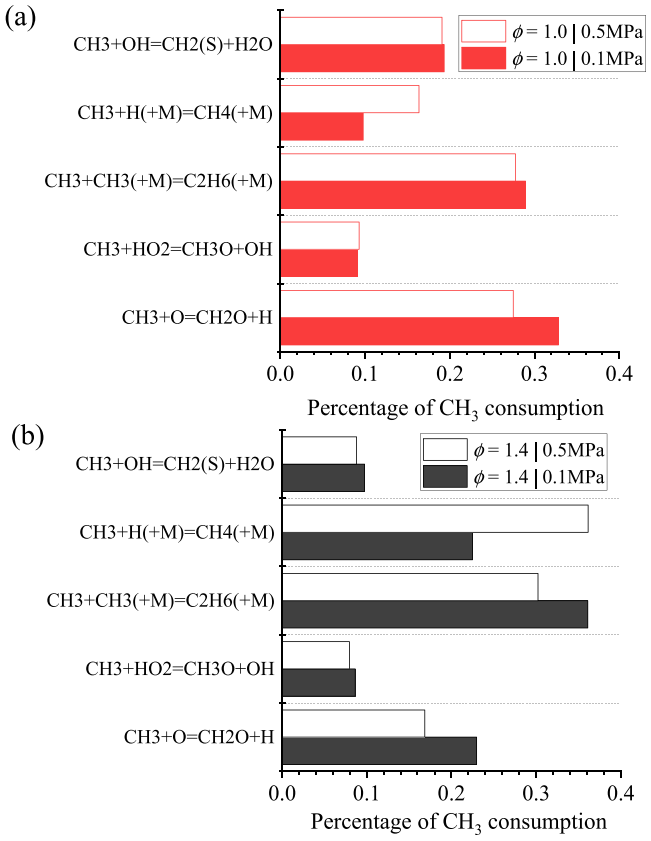

Fig. 16. Consumption percentage of CH_3 radical through different reactions for 60%DME fraction, P_u = 0.1 MPa and 0.5 MPa at (a) ϕ = 1.0 and (b) ϕ = 1.4.

The non-monotonic behavior of the power exponent β in DME fuels was not reported in previous studies. Goswami et al. [39] and Wang et al. [40] pointed out the reason why the non-monotonic behavior of β appears in CH_4 fuel, and they attributed it to the competition of reaction CH_3 + CH_3 (+M) = C_2H_6 (+M) and CH_3 + H (+M) = CH_4 (+M) in the rich side. Their finding is consistent with the asymptotic analysis of Seshadri et al. [65]. Therefore, similar to Konnov' viewpoint that the non-monotonic behavior of temperature power exponent α as a function of equivalence ratio could exist for all H/C/O fuels [66], the non-monotonic behavior of pressure power exponent β may also be expected for all H/C/O fuels.

The reaction pathways analysis and sensitivity analysis given above (see Figs. 12, 13, and 15) show that CH_3 radical is important and the non-monotonic behavior of β can be also associated with the competition between CH_3-containing reactions. Figure 16 shows the CH_3 consumption percentage of five most important CH_3-containing reactions in NH_3/DME/air flames for 60%DME frac-

tion, P_u = 0.1 MPa and 0.5 MPa at ϕ = 1.0 and 1.4. As the pressure increases, the three-body reaction $CH_3 + H (+M) = CH_4 (+M)$ enhances significantly in consumption of CH_3 radical for both stoichiometric combustion and rich burn. This is quite different from other CH_3 reactions. It also confirms the importance of the chain-termination reaction $CH_3 + H (+M) = CH_4 (+M)$ in decreasing laminar burning velocity with increasing initial pressure. When ϕ = 1.0, the main CH_3 consumption reactions are $CH_3 + O = CH_2O + H$ and $CH_3 + CH_3 (+M) = C_2H_6 (+M)$. $CH_3 + H (+M) = CH_4 (+M)$ as the important chain-termination reaction is less importance, and this indicates that the H radical consumption through this reaction is weak. When ϕ = 1.4, the main CH_3 consumption reactions convert to $CH_3 + H (+M) = CH_4 (+M)$ and $CH_3 + CH_3 (+M) = C_2H_6 (+M)$, and only these two reactions increase in consuming CH_3 with increasing equivalence ratio. This indicates that the H radical consumption through reaction $CH_3 + H (+M) = CH_4 (+M)$ is promoted on rich side. In addition, reaction $CH_3 + CH_3 (+M) = C_2H_6 (+M)$ in DME flames always dominates CH_3 consumption in stoichiometric combustion and rich side. This is different from that in CH_4 flames, that is the reaction $CH_3 + CH_3 (+M) = C_2H_6 (+M)$ only plays a dominant role in very rich flames. In other words, reaction $CH_3 + CH_3 (+M) = C_2H_6 (+M)$ in DME flames always restrains the rate of reaction $CH_3 + H (+M) = CH_4 (+M)$, especially at stoichiometric combustion. Furthermore, the promotion of reaction $CH_3 + H (+M) = CH_4 (+M)$ in consuming H radical with increasing ϕ enhances the competition with $H + O_2 = O + OH$, and leads to decrease in pressure power exponent β. This can explain the non-monotonic behavior of β (see Fig. 11).

Figure 17 shows the maximum mole fraction of NH_2 and CH_3 radical as a function of DME fraction for P_u = 0.1 MPa and 0.5 MPa at ϕ = 1.0 and 1.4. It can be seen that the maximum mole fraction of NH_2 decreases linearly with DME fraction for both stoichiometric combustion and rich burn when DME fraction is larger than 20%, while the maximum mole fraction of CH_3 always increases with increasing DME fraction. The slight increase of NH_2 for DME fraction < 20% means that a small amount DME addition can enhance the oxidation of NH_3, and this is attributed to the generation of H, OH, and O during the oxidation of DME. Furthermore, the intersections between the maximum mole fractions of NH_2 and CH_3 are within 30% - 40%DME for various conditions. This observation is consistent with the non-monotonic behavior of β with increasing equivalence ratio when DME fraction > ~40%. It corroborates that the monotonic behavior of β in high NH_3 content is due to the dominance of NH_2 recombination reactions, rather than CH_3, in decreasing the laminar burning velocity on the rich side. This agrees with the analysis by Wang et al. [15] in NH_3/CH_4/air flames.

To distinguish the key factors that lead to decrease in flame speed as pressure increases, here we analyze the thermal effect and chemical kinetics effect on laminar burning velocity. Figure 18 shows the numerical profiles of temperature (T) and mole fraction of O, H, and OH for NH_3/DME/air flames at 298 K, ϕ = 1.0, 20%, and 60%DME with different initial pressures (0.1, 0.3, and 0.5 MPa). It can be seen that the mole fractions of O, H, and OH decrease with the increase of initial pressure, and the decrease from 0.1 to 0.3 MPa is larger than that from 0.3 to 0.5 MPa. This is one reason for the negative dependence of laminar burning velocity on initial pressure (see Fig. 10) since the decrease of the chemical kinetics effect as pressure increases. Despite this, it cannot be denied that the increase of initial pressure can advance the reaction zone, which can be seen from the different peak positions of the same species in Fig. 18. In addition, the adiabatic flame temperatures at different initial pressures are quite close, i.e., for 20%DME, T_{ad} = 2160 K, 2190 K, and 2200 K at 0.1, 0.3, and 0.5 MPa, respectively, and for 60%DME, T_{ad} = 2240 K, 2270 K, and 2290 K at 0.1, 0.3, and 0.5 MPa, respectively, although the increase rate of temperature differs noticeably with initial pressure, especially for the pressure increase from 0.1 to 0.3 MPa. This implies the thermal effect has a minor influence on the laminar burning velocity as the initial pressure increases.

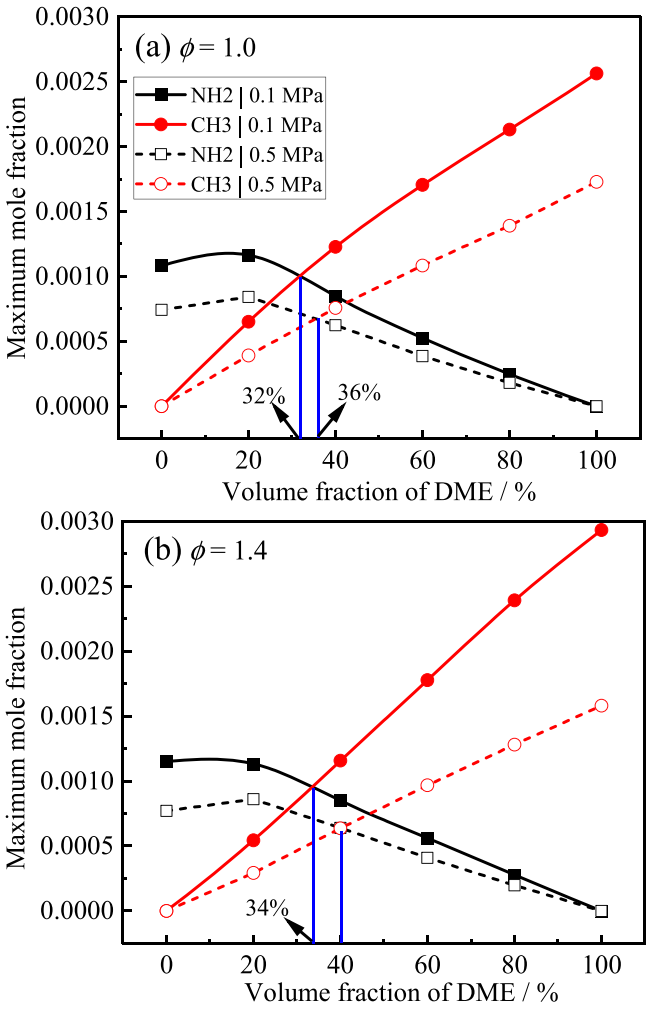

Fig. 17. The maximum mole fraction of NH_2 and CH_3 radical as a function of DME fraction for P_u = 0.1 MPa and 0.5 MPa at (a) ϕ = 1.0 and (b) ϕ = 1.4.

6. Conclusions

The laminar burning velocity of NH_3/DME/air flames with various DME fractions (0–100%DME) at 0.1 MPa, 298 K, and ϕ = 0.7–1.5 were studied using a spherical constant-volume combustion method and kinetic modeling. Pressure effect was also explored by considering different initial pressures (0.1, 0.3, and 0.5 MPa) for 20%–80%DME at 298 K and ϕ = 0.7–1.4.

A detailed reaction mechanism for the oxidation of NH_3/DME blends was developed and validated against experiments in this work. The predictions of the laminar burning velocity by the model developed are in good agreement with the experimental measurements for the NH_3/air, DME/air, and NH_3/DME/air mixtures. In addition, the model can well predict the ignition delay time of NH_3, DME, and NH_3/DME oxidation.

The results show that the laminar burning velocity of NH_3/DME/air mixtures increases linearly with increasing DME fraction, but decreases with increasing initial pressure. Detailed kinetic analyses performed using the reaction mechanism suggest that the positive effect of DME addition is mainly due to two reasons: (1) increased mole fraction of key free radicals such

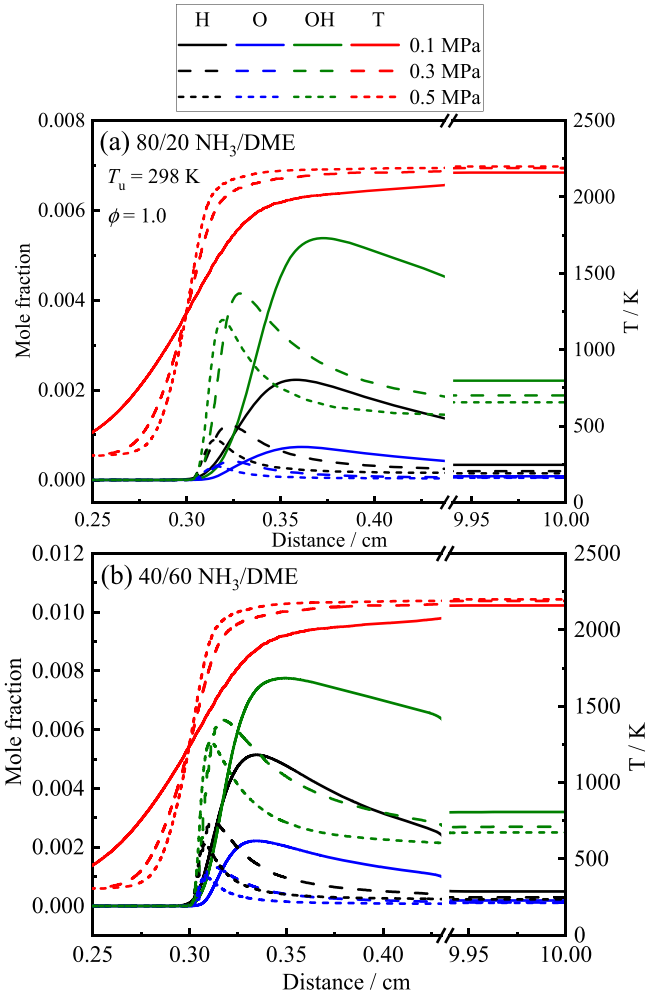

Fig. 18. Numerical profiles of temperature and mole fractions of O, H, and OH for NH_3/DME/air flames at T_u = 298 K, ϕ = 1.0, 20%DME, 60%DME, and different initial pressures, P_u = 0.1, 0.3, and 0.5 MPa.

as O, H, and OH, and (2) increased adiabatic flame temperature. The increase in DME fraction leads to an increased maximum mole fraction of the free radicals and thus causes an increase in laminar burning velocity. The increase in adiabatic flame temperature with increasing DME fraction results in an enhanced thermal effect and consequently promotes the burning process. Furthermore, the kinetic analysis indicates that the negative effect of pressure on laminar burning velocity is primarily due to the reduction of free radicals rather than the thermal effect.

The reaction pathways analysis shows that the main reaction pathways based on N-atom shift from routes (1) NH_3-NH_2-NH-N-N_2 and (3) NH_3-NH_2-(NH-N_2H_2)/ N_2H_2-NNH-N_2 to routes (1) NH_3-NH_2-NH-N-N_2 and (2) NH_3-NH_2-(NH-HNO)/ HNO-NO-(N_2)/N_2O-N_2 as DME fraction increases, whereas the main reaction pathways based on C-atom have minor variation.

The pressure power exponent β describing the dependence of the laminar burning velocity of NH_3/DME/air flames on pressure as a function of equivalence ratio shows different behaviors for different DME fractions. For DME fraction $<$ ~40%, β increases monotonic with equivalence ratio, but for DME fraction $>$ ~40%, it shows non-monotonic behavior. The non-monotonic behavior of β for high DME fractions can attribute to the enhancement of chain-termination reaction $CH_3 + H (+M) = CH_4 (+M)$ on the rich side. The monotonic behavior of β for low DME fractions is due to the fact that NH_2 recombination reactions play a greater role than CH_3 in decreasing laminar burning velocity. In addition, the results of sensitivity analysis between β and laminar burning velocity show a weak relevance, which confirms the statement that β can be an independent parameter for model validation.

This work provides fundamental measurements of the laminar burning velocity at various conditions and a kinetic model for NH_3/DME/air mixtures. Moreover, the insights gained from the kinetic analysis helped us further understand the NH_3/DME oxidation.

Declaration of Competing Interest

The authors declare that they have no known competing financial interests or personal relationships that could have appeared to influence the work reported in this paper.

Acknowledgments

This study was supported by the National Natural Science Foundation of China (Grant Nos. 51976210 and 52020105008), the DNL Cooperation Fund, CAS (DNL202006), and the Fundamental Research Funds for the Central Universities (Grant No. WK2320000055). The computing resources provided by the Supercomputing Center of University of Science and Technology of China is acknowledged.

Supplementary materials

Supplementary material associated with this article can be found, in the online version, at doi:10.1016/j.combustflame.2022.112372.

References

[1] A. Hayakawa, T. Goto, R. Mimoto, Y. Arakawa, T. Kudo, H. Kobayashi, Laminar burning velocity and Markstein length of ammonia/air premixed flames at various pressures, Fuel 159 (2015) 98–106.
[2] B.W. Mei, X.Y. Zhang, S.Y. Ma, M.L. Cui, H.W. Guo, Z.H. Cao, Y.Y. Li, Experimental and kinetic modeling investigation on the laminar flame propagation of ammonia under oxygen enrichment and elevated pressure conditions, Combust. Flame 210 (2019) 236–246.
[3] E.C. Okafor, Y. Naito, S. Colson, A. Ichikawa, T. Kudo, A. Hayakawa, H. Kobayashi, Experimental and numerical study of the laminar burning velocity of CH4–NH3–air premixed flames, Combust. Flame 187 (2018) 185–198.
[4] V.F. Zakaznov, L.A. Kursheva, Z.I. Felina, Determination of normal flame velocity and critical diameter of flame extinction in ammonia–air mixture, Combust. Explo. Shock+ 14 (1978) 710–713.
[5] P.D. Ronney, Effect of chemistry and rransport properties on near-limit flames at microgravity, Combust. Sci. Technol. 59 (1988) 123–141.
[6] T. Jabbour, D.F. Clodic, J. Terry, S. Kondo, Burning velocity and refrigerant flammability classification, Ashrae Transacti 110 (2004) 522–533.
[7] X. Han, Z. Wang, M. Costa, Z. Sun, Y. He, K. Cen, Experimental and kinetic modeling study of laminar burning velocities of NH_3/air, NH_3/H_2/air, NH_3/CO/air and NH3/CH4/air premixed flames, Combust. Flame 206 (2019) 214–226.
[8] C. Lhuillier, P. Brequigny, N. Lamoureux, F. Contino, C. Mounaïm-Rousselle, Experimental investigation on laminar burning velocities of ammonia/hydrogen/air mixtures at elevated temperatures, Fuel 263 (2020).
[9] E. Hu, X. Li, X. Meng, Y. Chen, Y. Cheng, Y. Xie, Z. Huang, Laminar flame speeds and ignition delay times of methane–air mixtures at elevated temperatures and pressures, Fuel 158 (2015) 1–10.
[10] Z. Chen, On the accuracy of laminar flame speeds measured from outwardly propagating spherical flames: methane/air at normal temperature and pressure, Combust. Flame 162 (2015) 2442–2453.
[11] X. Han, Z. Wang, Y. He, S. Wang, Y. Zhu, A.A. Konnov, Over-rich combustion of CH4, C2H6, and C3H8 +air premixed flames investigated by the heat flux method and kinetic modeling, Combust. Flame 210 (2019) 339–349.
[12] Z. Wang, X. Han, Y. He, R. Zhu, Y. Zhu, Z. Zhou, K. Cen, Experimental and kinetic study on the laminar burning velocities of NH3 mixing with CH_3OH and C_2H_5OH in premixed flames, Combust. Flame 229 (2021).
[13] G. Dayma, F. Halter, P. Dagaut, New insights into the peculiar behavior of laminar burning velocities of hydrogen–air flames according to pressure and equivalence ratio, Combust. Flame 161 (2014) 2235–2241.
[14] E.C. Okafor, Y. Naito, S. Colson, A. Ichikawa, T. Kudo, A. Hayakawa, H. Kobayashi, Measurement and modelling of the laminar burning velocity of methane-ammonia-air flames at high pressures using a reduced reaction mechanism, Combust. Flame 204 (2019) 162–175.

[15] S. Wang, Z. Wang, C. Chen, A.M. Elbaz, Z. Sun, W.L. Roberts, Applying heat flux method to laminar burning velocity measurements of NH3/CH4/air at elevated pressures and kinetic modeling study, Combust. Flame 236 (2022).

[16] K.P. Shrestha, C. Lhuillier, A.A. Barbosa, P. Brequigny, F. Contino, C. Mounaïm-Rousselle, L. Seidel, F. Mauss, An experimental and modeling study of ammonia with enriched oxygen content and ammonia/hydrogen laminar flame speed at elevated pressure and temperature, Proc. Combust. Inst. 38 (2021) 2163–2174.

[17] S. Wiseman, M. Rieth, A. Gruber, J.R. Dawson, J.H. Chen, A comparison of the blow-out behavior of turbulent premixed ammonia/hydrogen/nitrogen-air and methane–air flames, Proc. Combust. Inst. 38 (2021) 2869–2876.

[18] L. Dai, S. Gersen, P. Glarborg, H. Levinsky, A. Mokhov, Experimental and numerical analysis of the autoignition behavior of NH3 and NH3/H2 mixtures at high pressure, Combust. Flame 215 (2020) 134–144.

[19] A. Ichikawa, A. Hayakawa, Y. Kitagawa, K.D. Kunkuma Amila Somarathne, T. Kudo, H. Kobayashi, Laminar burning velocity and Markstein length of ammonia/hydrogen/air premixed flames at elevated pressures, Int. J. Hydrog. Energy 40 (2015) 9570–9578.

[20] X.L. Han, Z.H. Wang, Y. He, Y.Q. Zhu, K.F. Cen, Experimental and kinetic modeling study of laminar burning velocities of NH3/syngas/air premixed flames, Combust. Flame 213 (2020) 1–13.

[21] Z. Chen, Y. Jiang, Numerical investigation of the effects of H2/CO/syngas additions on laminar premixed combustion characteristics of NH3/air flame, Int. J. Hydrog. Energy 46 (2021) 12016–12030.

[22] A.M. Elbaz, S. Wang, T.F. Guiberti, W.L. Roberts, Review on the recent advances on ammonia combustion from the fundamentals to the applications, Fuel Communications 10 (2022).

[23] G. Issayev, B.R. Giri, A.M. Elbaz, K.P. Shrestha, F. Mauss, W.L. Roberts, A. Farooq, Ignition delay time and laminar flame speed measurements of ammonia blended with dimethyl ether: a promising low carbon fuel blend, Renew. Energ. 181 (2022) 1353–1370.

[24] L. Dai, H. Hashemi, P. Glarborg, S. Gersen, P. Marshall, A. Mokhov, H. Levinsky, Ignition delay times of NH_3 /DME blends at high pressure and low DME fraction: RCM experiments and simulations, Combust. Flame 227 (2021) 120–134.

[25] G. Issayev, B.R. Giri, A.M. Elbaz, K.P. Shrestha, F. Mauss, W.L. Roberts, A. Farooq, Combustion behavior of ammonia blended with diethyl ether, Proc. Combust. Inst. 38 (2021) 499–506.

[26] K.P. Shrestha, B.R. Giri, A.M. Elbaz, G. Issayev, W.L. Roberts, L. Seidel, F. Mauss, A. Farooq, A detailed chemical insights into the kinetics of diethyl ether enhancing ammonia combustion and the importance of NOx recycling mechanism, Fuel Communications 10 (2022).

[27] A.M. Elbaz, B.R. Giri, G. Issayev, K.P. Shrestha, F. Mauss, A. Farooq, W.L. Roberts, Experimental and kinetic modeling study of laminar flame speed of dimethoxymethane and ammonia blends, Energy Fuel 34 (2020) 14726–14740.

[28] C.W. Gross, S.C. Kong, Performance characteristics of a compression-ignition engine using direct-injection ammonia–DME mixtures, Fuel 103 (2013) 1069–1079.

[29] G. Yin, J. Li, M. Zhou, J. Li, C. Wang, E. Hu, Z. Huang, Experimental and kinetic study on laminar flame speeds of ammonia/dimethyl ether/air under high temperature and elevated pressure, Combust. Flame 238 (2022).

[30] P. Dagaut, P. Glarborg, M. Alzueta, The oxidation of hydrogen cyanide and related chemistry, Prog. Energy Combust. Sci. 34 (2008) 1–46.

[31] H. Nakamura, S. Hasegawa, T. Tezuka, Kinetic modeling of ammonia/air weak flames in a micro flow reactor with a controlled temperature profile, Combust. Flame 185 (2017) 16–27.

[32] J. Otomo, M. Koshi, T. Mitsumori, H. Iwasaki, K. Yamada, Chemical kinetic modeling of ammonia oxidation with improved reaction mechanism for ammonia/air and ammonia/hydrogen/air combustion, Int. J. Hydrog. Energy 43 (2018) 3004–3014.

[33] O. Mathieu, E.L. Petersen, Experimental and modeling study on the high-temperature oxidation of Ammonia and related NOx chemistry, Combust. Flame 162 (2015) 554–570.

[34] K.P. Shrestha, L. Seidel, T. Zeuch, F. Mauss, Detailed kinetic mechanism for the oxidation of ammonia including the formation and reduction of nitrogen oxides, Energy Fuel 32 (2018) 10202–10217.

[35] X. Zhang, S.P. Moosakutty, R.P. Rajan, M. Younes, S.M. Sarathy, Combustion chemistry of ammonia/hydrogen mixtures: Jet-stirred reactor measurements and comprehensive kinetic modeling, Combust. Flame 234 (2021).

[36] Z. Zhao, M. Chaos, A. Kazakov, F.L. Dryer, Thermal decomposition reaction and a comprehensive kinetic model of dimethyl ether, Int. J. Chem. Kinet. 40 (2008) 1–18.

[37] M. Goswami, R.J.M. Bastiaans, L.P.H. de Goey, A.A. Konnov, Experimental and modelling study of the effect of elevated pressure on ethane and propane flames, Fuel 166 (2016) 410–418.

[38] M. Metghalchi, J.C. Keck, Burning velocities of mixtures of air with methanol, isooctane, and indolene at high pressure and temperature, Combust. Flame 48 (1982) 191–210.

[39] M. Goswami, S.C.R. Derks, K. Coumans, W.J. Slikker, M.H. de Andrade Oliveira, R.J.M. Bastiaans, C.C.M. Luijten, L.P.H. de Goey, A.A. Konnov, The effect of elevated pressures on the laminar burning velocity of methane+air mixtures, Combust. Flame 160 (2013) 1627–1635.

[40] S. Wang, Z. Wang, Y. He, X. Han, Z. Sun, Y. Zhu, M. Costa, Laminar burning velocities of $CH_4/O_2/N_2$ and oxygen-enriched $CH_4/O_2/CO_2$ flames at elevated pressures measured using the heat flux method, Fuel 259 (2020).

[41] H. Li, H. Xiao, J. Sun, Laminar burning velocity, Markstein length, and cellular instability of spherically propagating NH3 /H2 /Air premixed flames at moderate pressures, Combust. Flame 241 (2022) 112079.

[42] D. Bradley, P.H. Gaskell, X.J. Gu, Burning velocities, markstein lengths, and flame quenching for spherical methane-air flames: a computational study, Combust. Flame 104 (1996) 176–198.

[43] S.Y. Liao, D.M. Jiang, J. Gao, Z.H. Huang, Q. Cheng, Measurements of Markstein numbers and laminar burning velocities for liquefied petroleum gas–air mixtures, Fuel 83 (2004) 1281–1288.

[44] Z. Huang, Y. Zhang, K. Zeng, B. Liu, Q. Wang, D. Jiang, Measurements of laminar burning velocities for natural gas–hydrogen–air mixtures, Combust. Flame 146 (2006) 302–311.

[45] M.P. Burke, Z. Chen, Y. Ju, F.L. Dryer, Effect of cylindrical confinement on the determination of laminar flame speeds using outwardly propagating flames, Combust. Flame 156 (2009) 771–779.

[46] D. Bradley, R.A. Hicks, M. Lawes, C.G.W. Sheppard, R. Woolley, The measurement of laminar burning velocities and Markstein numbers for Iso-octane–air and Iso-octane–n-Heptane–air mixtures at elevated temperatures and pressures in an explosion bomb, Combust. Flame 115 (1998) 126–144.

[47] A.P. Kelley, C.K. Law, Nonlinear effects in the extraction of laminar flame speeds from expanding spherical flames, Combust. Flame 156 (2009) 1844–1851.

[48] CHEMKIN-PRO17.0 Release 15151, ANSYS Reaction Design, San Diego, 2016.

[49] Z. Chen, C. Tang, J. Fu, X. Jiang, Q. Li, L. Wei, Z. Huang, Experimental and numerical investigation on diluted DME flames: thermal and chemical kinetic effects on laminar flame speeds, Fuel 102 (2012) 567–573.

[50] H. Yu, E. Hu, Y. Cheng, X. Zhang, Z. Huang, Experimental and numerical study of laminar premixed dimethyl ether/methane–air flame, Fuel 136 (2014) 37–45.

[51] K.P. Shrestha, S. Eckart, A.M. Elbaz, B.R. Giri, C. Fritsche, L. Seidel, W.L. Roberts, H. Krause, F. Mauss, A comprehensive kinetic model for dimethyl ether and dimethoxymethane oxidation and NO interaction utilizing experimental laminar flame speed measurements at elevated pressure and temperature, Combust. Flame 218 (2020) 57–74.

[52] Q.S. Li, R.H. Lu, Direction dynamics study of the hydrogen abstraction reaction CH2O + NH2 → CHO + NH3, J. Phys. Chem. A 106 (2002) 9446–9450.

[53] J.T. Jodkowski, E. Ratajczak, K. Fagerstrom, A. Lund, N.D. Stothard, R. Humpfer, H.H. Grotheer, Kinetics of the cross reaction between amidogen and methyl radicals, Chem. Phys. Lett. 240 (1995) 63–71.

[54] P. Glarborg, C.S. Andreasen, H. Hashemi, R. Qian, P. Marshall, Oxidation of methylamine, Int. J. Chem. Kinet. 52 (2020) 893–906.

[55] G. Capriolo, C. Brackmann, M. Lubrano Lavadera, T. Methling, A.A. Konnov, An experimental and kinetic modeling study on nitric oxide formation in premixed C3 alcohols flames, Proc. Combust. Inst. 38 (2021) 805–812.

[56] U. Burke, K.P. Somers, P. O'Toole, C.M. Zinner, N. Marquet, G. Bourque, E.L. Petersen, W.K. Metcalfe, Z. Serinyel, H.J. Curran, An ignition delay and kinetic modeling study of methane, dimethyl ether, and their mixtures at high pressures, Combust. Flame 162 (2015) 315–330.

[57] G.P. Smith, D.M. Golden, M. Frenklach, N.W. Moriarty, B. Eiteneer, M. Goldenberg, GRI-Mech 3.0. Gas Research Institute, available at http://www.me.berkeley.edu/gri_mech/.

[58] C.A. Daly, J.M. Simmie, J. Würmel, N. Djebaĭli, C. Paillard, Burning velocities of dimethyl ether and air, Combust. Flame 125 (2001) 1329–1340.

[59] X. Qin, Y. Ju, Measurements of burning velocities of dimethyl ether and air premixed flames at elevated pressures, Proc. Combust. Inst. 30 (2005) 233–240.

[60] Y.L. Wang, A.T. Holley, C. Ji, F.N. Egolfopoulos, T.T. Tsotsis, H.J. Curran, Propagation and extinction of premixed dimethyl-ether/air flames, Proc. Combust. Inst. 32 (2009) 1035–1042.

[61] W.S. Song, S.W. Jung, J. Park, O.B. Kwon, Y.J. Kim, T.H. Kim, J.H. Yun, S.I. Keel, Effects of syngas addition on flame propagation and stability in outwardly propagating spherical dimethyl ether-air premixed flames, Int. J. Hydrog. Energy 38 (2013) 14102–14114.

[62] S. Wang, Z. Wang, A.M. Elbaz, X. Han, Y. He, M. Costa, A.A. Konnov, W.L. Roberts, Experimental study and kinetic analysis of the laminar burning velocity of NH3/syngas/air, NH3/CO/air and NH3/H2/air premixed flames at elevated pressures, Combust. Flame 221 (2020) 270–287.

[63] F.N. Egolfopoulos, C.K. Law, Chain mechanisms in the overall reaction orders in laminar flame propagation, Combust. Flame 80 (1990) 7–16.

[64] X. Meng, M. Zhang, C. Zhao, H. Tian, J. Tian, W. Long, M. Bi, Study of combustion and NO chemical reaction mechanism in ammonia blended with DME, Fuel 319 (2022).

[65] K. Seshadri, X.S. Bai, H. Pitsch, Asymptotic structure of rich methane-air flames, Combust. Flame 127 (2001) 2265–2277.

[66] A.A. Konnov, The effect of temperature on the adiabatic laminar burning velocities of CH4−air and H2−air flames, Fuel 89 (2010) 2211–2216.